CFP was diffusely distributed in a pan-cellular manner (Fig. 5K). However, foci formation took place inside the nucleus when forskolin was added. In this case, not only GCN5 and Ad4BP/SF-1 were colocalized in fluorescent dots, but TRRAP also made foci and finely colocalized with GCN5 and Ad4BP/SF-1 (Fig. 5L). These data suggest that PKA activation assembles Ad4BP/SF-1 into foci with an accompanying recruitment of coactivators like the GCN5/TRRAP complex.

DAX-1 Immobilized Ad4BP/SF-1 in the Nucleus, and this Process Was Rescued by PKA

DAX-1 is a suppressive protein for the transcriptional activation induced by Ad4BP/SF-1 and is thus considered to be an inhibitor of steroidogenesis. It has been proved that DAX-1 can bind directly to Ad4BP/SF-1 and antagonize the transcriptional activity of Ad4BP/SF-1, either via its silencing C-terminal domain (31) or by recruiting the corepressors N-CoR (11) or Alien (32) to Ad4BP/SF-1. We investigated the relationship between DAX-1 and Ad4BP/SF-1 during the process of activation of Ad4BP/SF-1 induced by PKA. The dual-luciferase assay revealed that the inhibition of the transcriptional activity of Ad4BP/SF-1 induced by DAX-1 could be recovered by PKA stimulation (Fig. 6). Next, the subcellular distributions of GFP-DAX-1 alone, and combined with YFP-Ad4BP/SF-1, were studied in living KGN cells the PKA signal pathway of which was either blocked or activated. When the cells were transfected by GFP-DAX-1 alone, the fluorescence signal was predominantly located in the nucleus in a homogenous manner, while a relatively weak diffuse fluorescence was observed in the cytosol (Fig. 7A). Forskolin (10^{-6} mol/liter) treatment caused no effect on this distribution pattern of DAX-1 (Fig. 7B). The same distribution pattern of endogenous DAX-1 in KGN cells was observed by immunostaining (data not shown). However, cotransfection of GFP-DAX-1 and YFP-Ad4BP/SF-1 caused a dramatic change in the subcellular distribution patterns. Namely, both proteins assembled to form clear dots with no visible diffuse fluorescent background, and the GFP-DAX-1 and YFP-Ad4BP/SF-1 fluorescent dots completely overlapped (Fig. 7C, i, ii, and iii). This was further supported by the LSM semiquantitative colocalization analysis (Fig. 7C, iv). The weak GFP signal observed in the cytosol when GFP-DAX-1 was solely transfected also completely disappeared (Fig. 7C). More importantly, the completely overlapping GFP-DAX-1 and YFP-Ad4BP/SF-1 fluorescence signals were partially separated when the cells were stimulated by 10^{-6} mol/liter forskolin (Fig. 7D). The LSM colocalization analysis showed that the incomplete colocalization resulted from partial GFP-DAX-1 signal being disassociated from the overlapping dots (Fig. 7D, iv). This phenomenon was observed in most cells with proper expression of both GFP-DAX-1 and YFP-Ad4BP/SF-1, although it has been observed that different individual cells respond to forskolin stimulation to a variable extent (data not shown). Thus interaction between DAX-1 and Ad4BP/SF-1 might be interfered with or weakened by activation of PKA, and DAX-1 might be stripped from binding with Ad4BP/SF-1 when PKA is activated.

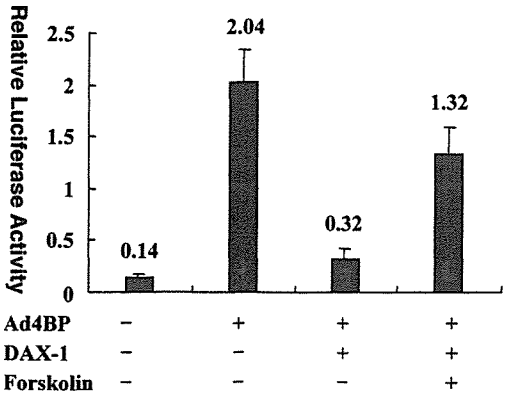

Fig. 6. Effect of Forskolin on DAX-1-Mediated Inhibition of Ad4BP/SF-1 Transactivation

KGN cells were cotransfected with pGL3-ArPII and phRL-CMV. The strategy for cotransfection of Ad4BP/SF-1, DAX-1, or both, and the treatment with forskolin are indicated. DAX-1 could repress Ad4BP/SF-1-mediated transcription, whereas the DAX-1-inhibited Ad4BP/SF-1 transactivation could be rescued by forskolin.

To further investigate this hypothesis, we applied the FRAP technique to examine the intranuclear dynamics of fluorescent Ad4BP/SF-1 and DAX-1 in living KGN cells. Proper mobility has recently been shown to be important for nuclear receptors to be transactivationally functional (21). As shown in Fig. 8, coexpression of pRc/RSV-DAX-1 not only changed the subnuclear distribution pattern of YFP-Ad4BP/SF-1, but also clearly immobilized YFP-Ad4BP/SF-1. When PKA was blocked, the half-maximal recovery time ($t_{1/2}$) of YFP-Ad4BP/SF-1 with no cotransfection of DAX-1 was 0.84 ± 0.16 sec (mean ± SD, n =20, Fig. 8A), whereas the recovery $t_{1/2}$ of YFP-Ad4BP/SF-1 with cotransfection of DAX-1 was prolonged to 9.21 ± 2.36 sec (mean ± SD, n =20, Fig. 8B). These data strongly suggest that Ad4BP/SF-1 is quite mobile in the nucleus, and interaction of the receptor with DAX-1 may interfere with its mobility. Immobilization of Ad4BP/SF-1 might also be a mechanism through which DAX-1 exerts its inhibitory effect on Ad4BP/SF-1, in addition to the mechanism of direct interaction and recruitment of corepressors. We further studied the mobility of YFP-Ad4BP/SF-1 with the coexpression of DAX-1 with forskolin to activate the intracellular PKA pathway. Interestingly, the sharply reduced mobility of YFP-Ad4BP/SF-1 induced by DAX-1 partially recovered in the presence of forskolin (recovery $t_{1/2}$: 1.78 ± 0.34 sec, mean ± SD, n =20, Fig. 8C). From these data, activation of PKA might be able to disrupt or weaken the direct interaction of the inhibitory DAX-1 with Ad4BP/SF-1 and thus potentiate the transactivation

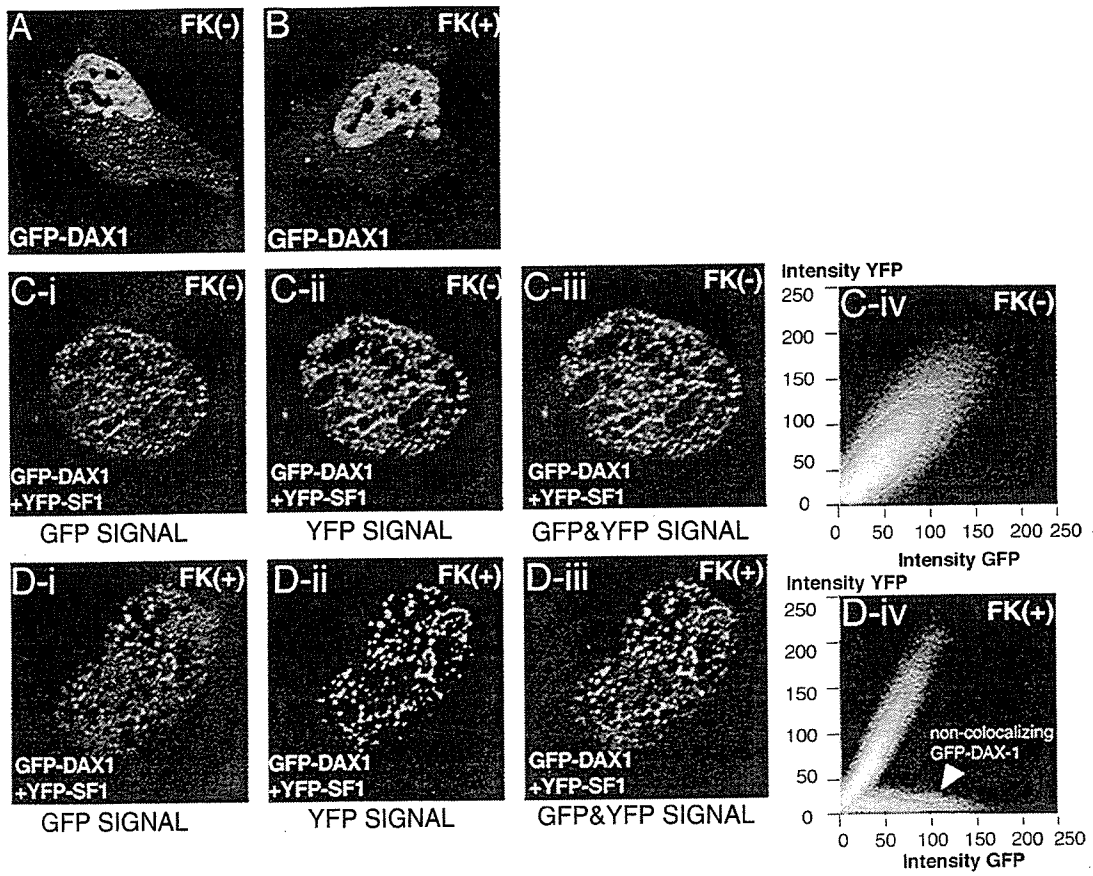

Fig. 7. Subcellular Distribution Interaction between GFP-DAX-1 and YFP-Ad4BP/SF-1

KGN cells were transfected with GFP-DAX-1 or GFP-DAX-1 + YFP-Ad4BP/SF-1 as indicated in each panel. A and B, DAX-1 is mainly diffuse in the nucleus with a weak signal detected in the cytoplasm, and this distribution is not altered by forskolin. C, Coexistence of GFP-DAX-1 and YFP-Ad4BP/SF-1 leads to the formation of clear dots with both fluorescent signals overlapping each other. The LSM colocalization analysis (C-iv) shows that GFP-DAX-1 and YFP-Ad4BP/SF-1 signals are colocalizing almost completely. No diffuse intranuclear fluorescence background or weak cytosol fluorescence was detected. D, Forskolin partially separated the two completely overlapping fluorescent signals The colocalization analysis (D-iv) shows that a fraction of GFP-DAX-1 signal is not colocalizing with YFP-Ad4BP/SF-1, suggesting that the interaction between Ad4BP/SF-1 and DAX-1 is weakened, and partial DAX-1 is disassociated from the Ad4BP/SF-1-DAX-1 binding complex.

of Ad4BP/SF-1, as shown by the luciferase reporter assay in Fig. 6.

DISCUSSION

Various lipophilic ligands have been found to interact with ligand-binding domains, induce allosteric changes, and thus convert nuclear receptors into an active conformation that can actively regulate transcription. However, Ad4BP/SF-1 is an orphan nuclear receptor and has no known ligand. Cross-talk with the main intracellular signal transduction pathways and protein-protein interactions seem to play definitive roles in the transcriptional regulation by nuclear receptors, especially those orphan nuclear receptors like Ad4BP/SF-1.

It is well known that the transactivational activity of Ad4BP/SF-1 can be further activated by the cAMP-PKA signal pathway. In this study, this phenomenon was also observed in a well known Ad4BP/SF-1 target gene's promoter, *human CYP19* ArPII, in KGN cells. The precise mechanism by which cAMP potentiates Ad4BP/SF-1-dependent transactivation was investigated using this model. One hypothesis is that PKA may directly or indirectly activate Ad4BP/SF-1 transcriptional activity by phosphorylation of Ad4BP/SF-1 because Ad4BP/SF-1 has been demonstrated to be phosphorylated *in vitro* by the PKA or MAPK pathway (33, 34). However, mutations of the predicted potential phosphorylation sites for the PKA (Ser 430) and MAPK (Ser 203) pathways did not affect the ability of PKA to stimulate Ad4BP/SF-1-dependent transactivational activity (26). In fact, it was shown to be difficult to prove that elevated cAMP could stimulate the phosphorylation of Ad4BP/SF-1 *in vivo* (35). In this regard, the opposite theory has recently been proposed that during the process of PKA-mediated Ad4BP/SF-1

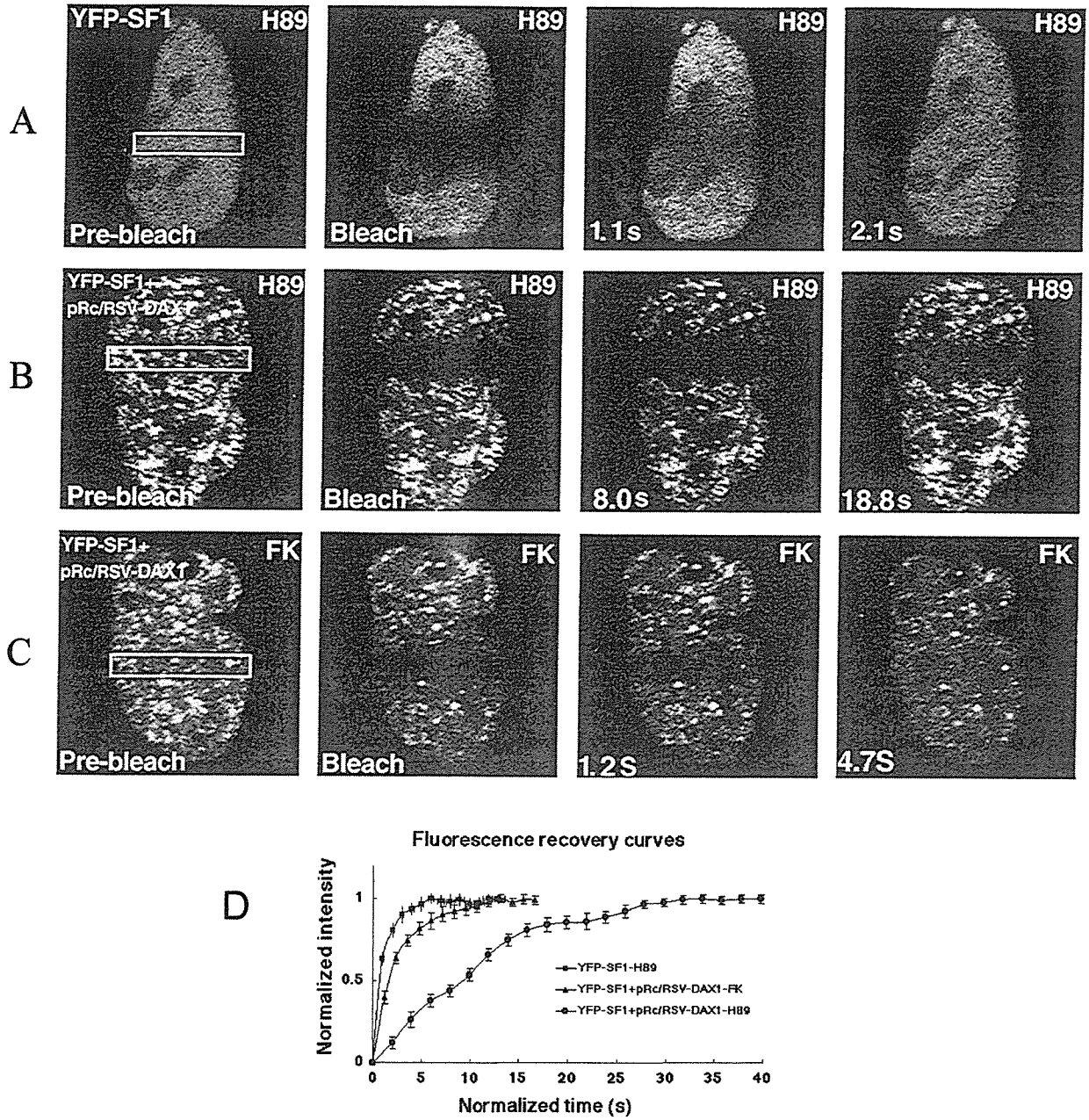

Fig. 8. FRAP Analysis of YFP-Ad4BP/SF-1 Cotransfected with pRc/RSV-DAX-1 after Forskolin or H89 Treatment

KGN cells were transfected with YFP-Ad4BP/SF-1 or YFP-Ad4BP/SF-1+ pRc/RSV-DAX-1, and treated with 10^{-6} mol/liter H89 or 10^{-6} mol/liter forskolin as indicated. Images show a single Z section and were obtained before and after bleaching at the time points indicated in each panel. The region of interest (ROI) of photobleaching is also indicated. A, When YFP-Ad4BP/SF-1 was solely transfected and cells were treated with H89, YFP-Ad4BP/SF-1 demonstrates a high intranuclear mobility. A definite bleach zone is detected after photobleaching. The total nuclear fluorescence reaches equilibrium within 1 sec. B, Cotransfection of pRc/RSV-DAX-1 and treatment with H89 prolonged the fluorescence recovery half-time to 9 sec, indicating that Ad4BP/SF-1 mobility is reduced. C, The prolonged fluorescence recovery time is rescued by forskolin. Ad4BP/SF-1 regains its mobility in the presence of forskolin, suggesting that PKA weakens the Ad4BP/SF-1-DAX-1 interaction. D, The recovery curves of the three groups of cells. The normalized intensity at each time point was averaged and plotted to the normalized time points. The $t_{1/2}$ value can be readily observed from the graph as the time at which the normalized intensity reaches 0.5 arbitrary units.

transactivation, phosphatase activity, but not kinase activity, may be critical (36). Another possible mechanism suggested was that PKA may increase the Ad4BP/SF-1 protein level by stabilizing it (26), but there is also conflicting evidence that the mRNA or protein level of Ad4BP/SF-1 remains constant after elevation or decrease of the cAMP level (37, 38). Peroxisome proliferators activated receptor-γ coactivator 1 (PGC-1) is an unique coactivator that can be transcriptionally increased by cAMP-PKA signaling (39).

The possibility that PKA may augment Ad4BP/SF-1 transactivation by means of increasing the PGC-1 level, if PGC-1 could serve as a coactivator for Ad4BP/SF-1, seems to be unlikely because forced expression of PGC-1 could not further enhance Ad4BP/SF-1-mediated ArPII activity in either KGN or NIH-3T3 cells (data not shown).

Ligand-induced subnuclear compartmentalization (foci formation) is a common phenomenon of non-orphan nuclear receptors and usually is considered to be related to the transactivationally active form of receptors. Ligand-induced transactivationally active GR (40), vitamin D receptor (41), estrogen receptor (ER) (42), mineralocorticoid receptor (43), and androgen receptor (AR) (44) have been found to be distributed in the nuclei that produce the GFP fluorescent foci. Intranuclear fluorescent foci formation depends closely on whether the receptor is transcriptionally active or inactive. Transcriptionally active AR treated with dihydrotestosterone produced 250–400 foci in the boundary region between euchromatin and heterochromatin (44). Although AR bound to antiandrogens like hydroxyflutamide also translocated to the nucleus, they spread homogeneously throughout the nucleus without producing any fluorescent foci (44). In addition, when ARs make foci, as induced by dihydrotestosterone, coactivators like SRC-1, TIF2, and CBP were found to be accumulated in identical locations, and CBP was found to be one of the factors essential for AR foci formation (25). It is thus speculated that transcriptionally activated nuclear receptors are transferred to common nuclear compartments (foci) in the nuclear matrix and form a complex with coactivators, and that this process is essential for full transactivation. However, it is unlikely that foci compartments directly represent the active transcription sites, because they were found usually not to overlap with activated RNA polymerase II or nascent mRNA. But currently, liganded GR has been observed to dynamically aggregate to an artificial promoter (a MMTV array that has been integrated to chromosome), where the biding sites are amplified many times (18, 19). Another corroborative study reported a strong correlation between aryl hydrocarbon receptor foci and the active transcription sites (45). Recent studies generally suggest that foci compartments of nuclear receptors may represent the sites for storage and/or assembly of activated nuclear receptor, and nuclear receptors can be dynamically recruited from foci compartments into the active transcription sites. It should be noted that foci are also possibly related to protein degradation compartment (46), because cognate ligand also induce proteolysis, a process that is tightly coupled with the ligand-induced activation and compartmentalization of nuclear receptors, and is believed to be a mechanism to precisely regulate the activity of liganded nuclear receptors.

In parallel with the elevated transactivation ability, GFP-Ad4BP/SF-1 underwent a compartmental shift and manifested foci formation in the nucleus when the PKA signal pathway was activated. This phenomenon was observed only with wild-type Ad4BP/SF-1, and not in the functionally inactive mutant Ad4BP/SF-1 (G35E). The PKA-inducible foci formation appears to be a characteristic of functionally stimulated Ad4BP/SF-1 because it is consistent with the PKA-stimulated transactivation of Ad4BP/SF-1, suggesting that Ad4BP/SF-1 is assembled to a transactivationally active subnuclear compartment. In addition, in the process of PKA-triggered foci formation, recruitment of coactivators such as GCN5 and TRRAP also takes place. It should be noted that this PKA-induced foci formation occurs on a diffuse fluorescence signal background, suggesting that not all Ad4BP/SF-1 proteins, but rather a fraction of them, are assembled to the foci, and that the Ad4BP/SF-1 in the nuclear pool may be undergoing rapid exchange.

The GCN5/TRRAP complex is a newly identified third class of nuclear receptor coactivator complex, in addition to the previously described P160/CBP HAT complex and vitamin D receptor-interacting protein/thyroid hormone receptor-associated protein non-HAT complex. GCN5 contains HAT activity whereas the three LXXLL motifs of TRRAP are responsible for interaction with nuclear receptors, according to the reported case of ERα, in a ligand-dependent manner (30). Based on our data, TRRAP is a surprisingly dominant cytoplasmic protein but seems to be dragged into the nucleus by its partner, GCN5. Both of these proteins can be recruited to Ad4BP/SF-1 when the receptor is stimulated by PKA, suggesting that this nuclear receptor coactivator complex is involved in the Ad4BP/SF-1 activation process. Therefore, activation of the PKA signal pathway is able to alter the subnuclear distribution pattern of Ad4BP/SF-1 and assemble this orphan nuclear receptor to a functionally active state, with recruitment of coactivators. Forskolin, a stimulator of adenyl cyclase, could induce Ad4BP/SF-1 to make foci, a phenomenon mimicking the role of cognate ligands to their respective nuclear receptors, raising a new concept that foci formation can also be a result of the activation of an intracellular signal pathway like PKA, which secondarily activates the nuclear receptors themselves. This result sheds new light on our understanding of the nature of foci, which has not yet been well defined.

The mutant Ad4BP/SF-1 (G35E) could not be transactivationally enhanced by PKA and could not make foci in the presence of forskolin. Surprisingly, however, mutant Ad4BP/SF-1 fluorescence aggregated in dots in the nucleoli. Although no significant nucleolar fluorescence was detectable in the case of the wild type, we cannot exclude the presence of a small fraction of Ad4BP/SF-1 molecules localizing to the nucleolus. The p-box of Ad4BP/SF-1, where the G35E mutation is located, or the region nearby, might be an important domain required for nuclear matrix binding of Ad4BP/SF-1 and thus prevent Ad4BP/SF-1 from entering the nucleoli, or this domain might be a nucleolus export

signal for the small fraction of Ad4BP/SF-1 that has entered the nucleolus to get out.

DAX-1 is able to interact directly with Ad4BP/SF-1 (31). The amino-terminal region of DAX-1 contains an interaction domain for Ad4BP/SF-1, and the C terminus of DAX-1 is itself transcriptionally silencing. In addition to the recruitment of corepressors like N-CoR, this silencing C terminus may be the second mechanism by which DAX-1 inhibits Ad4BP/SF-1 transactivation. This silencing carboxyl terminus also correlates with naturally occurring AHC mutations. Coexistence of GFP-DAX-1 and YFP-Ad4BP/SF-1 dramatically changed the fluorescence pattern of both proteins from diffuse distributions to the formation of clear dots, with the two fluorescence signals completely overlapping. The FRAP data in this study revealed that the intranuclear mobility of Ad4BP/SF-1 was also affected upon interaction with DAX-1.

Agonist-bound nuclear receptors form nuclear matrix-bound foci and are believed to be capable of undergoing rapid exchange. As an example, E2 treatment leads ER and the cofactor SRC-1 to strongly interact with the nuclear matrix, after which ER is partially immobilized, possibly representing interaction with more immobilized components of the nuclear structure. Ligand-bound ER and SRC-1 are still capable of rapid recovery within seconds of photobleaching. In the case of an ER antagonist, ER is extremely immobilized with no appreciable photobleaching recovery for several minutes at least, and this immobilization provides a new explanation for the inhibitory effects of the ER antagonist (21). The orphan receptor Ad4BP/SF-1 was also found to be quite mobile within the nucleus, with a mean recovery $t_{1/2}$ of around 0.8 sec after photobleaching. DAX-1 had a very different effect on Ad4BP/SF-1 with respect to the intranuclear mobility. Coexpression of DAX-1 resulted in clearly reduced mobility of Ad4BP/SF-1. These data, together with the result that Ad4BP/SF-1 and DAX-1 undergo the formation of colocalized dots upon interacting with each other, suggest that Ad4BP/SF-1 might be tightly bound to some special structure in the nuclear matrix upon binding with DAX-1. DAX-1 might work as an anchor protein mediating the sharp immobilization of Ad4BP/SF-1 in the nuclear matrix structure. Protein-protein interaction might affect the intracellular mobility of some steroid receptor and thereby contribute to their biological activity.

However, forskolin treatment enabled Ad4BP/SF-1 to recover from the transactivation suppression induced by DAX-1 as evidenced by the luciferase assay and by the fact that the complete overlapping of Ad4BP/SF-1 and DAX-1 signals was partially separated upon PKA activation. This was further supported by the FRAP data showing that the DAX-1-reduced mobility of Ad4BP/SF-1 was rescued by the activation of PKA. These data collectively suggest that activation of PKA may weaken the interaction between DAX-1 and Ad4BP/SF-1 and may disassemble DAX-1 from Ad4BP/SF-1, thus leading to the recovery of Ad4BP/SF-1 transcriptional activity. A previous study also demonstrated that the presence or absence of DAX-1 could not change the SF-1-SF-1-responsive element EMSA result (31). This means that, although DAX-1 can bind directly to SF-1, when SF-1 is activated and binds to the promoters of target genes, it is SF-1 alone, not in combination with DAX-1, that binds to the DNA, *i.e.* DAX-1 must now be stripped from binding with SF-1.

In the Ad4BP/SF-1 amino acid sequence, two regions were determined to be important for the interaction with DAX-1 (11). One is termed the R domain, which is between amino acids 437 and 447, and the other is residue 226 to 230 (ELILQ) of Ad4BP/SF-1. It is intriguing that the interaction between Ad4BP/SF-1 and the coactivator SRC-1 also requires the same residues (ELILQ), leading to the logical deduction that Ad4BP/SF-1-DAX-1 binding and Ad4BP/SF-1-coactivator binding may be mutually competitive, *i.e.* the Ad4BP/SF-1-interacting coactivator-repressor balance may determine the transactivation ability of Ad4BP/SF-1. Based on our present study, activation of the PKA signal pathway leads to the recruitment of the GCN5/TRRAP coactivator complex, and also to the disassembly of the inhibitory DAX-1, both of which may finally direct the coactivator-repressor balance to favoring the activation of Ad4BP/SF-1.

Collectively, activation of PKA can assemble Ad4BP/SF-1 to an active state, as manifested by foci formation, and this process is accompanied by the recruitment of coactivators GCN5/TRRAP, which might represent a newly identified cofactor complex for Ad4BP/SF-1. Direct interaction between Ad4BP/SF-1 and the repressor DAX-1 was visualized as completely overlapping fluorescent dots, and DAX-1 sharply immobilized Ad4BP/SF-1 upon binding. Activation of PKA was able to disrupt or weaken the interaction between DAX-1 and Ad4BP/SF-1 and therefore rescue the Ad4BP/SF-1 transactivation capability. In conclusion, activation of PKA may reintegrate the protein-protein interactions between Ad4BP/SF-1 and its coactivators and repressor, which finally decide the Ad4BP/SF-1 transactivation capability.

MATERIALS AND METHODS

Cell Culture

The human ovarian granulosa-like tumor cell line KGN was originally established by our group and expresses a high level of aromatase activity that is PKA dependent (47); the cells also highly express Ad4BP/SF-1 (48). The cells were maintained in DMEM/Nutrient Mixture F-12, Life Technologies, Inc., Gaithersburg, MD) supplemented with 10% fetal bovine serum, 10 U/liter penicillin, and 10 μg/ml streptomycin in an atmosphere of 5% CO_2 at 37 C. NIH-3T3 and CV1 cells were obtained from American Type Culture Collection (Manassas, VA) and maintained in DMEM supplemented with 10% fetal bovine serum, 10 U/liter penicillin and 10 μg/ml streptomycin in 75-cm^2 flasks at 37 C in 5% CO_2.

Plasmid Constructions

A full-length human Ad4BP/SF-1 cDNA was cloned from a human spleen cDNA library (BD Bioscience CLONTECH, Palo Alto, CA) by PCR using primers based on the human Ad4BP/SF-1 cDNA sequence (GenBank accession no. NM 004959.2). The PCR was performed using an Advantage cDNA PCR kit (BD Bioscience CLONTECH) and an automated thermo-cycler (Whatman Biometra, Gottingen, Germany) with the appropriate program. The PCR product was first subcloned into the pGEM-T-Easy vector (Promega Corp., Madison, WI) and sequenced to validate its structure using an ABI PRIM 377 DNA sequencer (PE Applied Biosystems, Foster City, CA). Finally, Ad4BP/SF-1 cDNA was subcloned into the expression vector pcDNA3.1 (+) (Invitrogen, San Diego, CA) at the *Not*I and *Xba*I restriction sites to produce pcDNA 3.1-Ad4BP/SF-1.

A mutant human Ad4BP/SF-1 cDNA construct containing the G35E mutation found in the patient (8) was made using a QuikChange site-directed mutagenesis kit (Stratagene, La Jolla, CA). Full-length cDNAs of wild-type and mutant Ad4BP/SF-1 were then subcloned into the *Sac*II sites of both pEGFP-C1 and pEYFP-C1 (CLONTECH Laboratories, Inc.), downstream of the humanized GFP or YFP sequence. The boundary regions between GFP (or YFP) and the human Ad4BP/SF-1 cDNAs were sequenced to validate that the Ad4BP/SF-1 cDNAs were placed in the reading frame of GFP or YFP. A human full-length DAX-1 expression vector pRc/RSV-DAX-1 was prepared as previously described (49). The expression plasmids for GFP-DAX-1 chimeras were constructed by inserting the full-length DAX-1 cDNA into the *Hin*dIII and *Xba*I sites of pEGFP-C3 (CLONTECH Laboratories, Inc.). Expression vectors pcDNA3-GCN5 and pcDNA3-TRRAP were constructed previously (30). To make GFP-GCN5, the full-length GCN5 cDNA was inserted into the *Eco*RI-*Xba*I sites of pEGFP-C2, downstream of the fluorescence protein. Chimeras for TRRAP-GFP, TRRAP-YFP, and TRRAP-CFP were prepared by inserting the full-length TRRAP cDNA into the *Eco*RI site of pEGFP-N1, pEYFP-N1, and pECFP-N1, respectively, in which TRRAP was fused to the N terminus of the fluorescent proteins. The firefly luciferase reporter vector pGL3-ArPII construct containing a 1.0-kb human cytochrome P450 CYP19 ArPII was described previously (50).

Relative Luciferase Reporter Assay

On the first day, 1.5×10^5 cells per well in 1 ml growth medium were seeded into 12-well plates. On the second day, 0.8 μg of PGL3-ArPII, 2.0 ng of phRL-CMV, and a total amount of 0.15μg of expression vectors for human Ad4BP/SF-1, chimerical fluorescent protein-Ad4BP/SF-1, or Ad4BP/SF-1 plus other plasmids such as DAX-1, GCN5, TRRAP, or their fluorescent protein chimerical plasmids were transiently cotransfected to each well using the Superfect transfection reagent (QIAGEN, Valencia, CA) following the manufacturer's protocol. For coexpression studies, the total amount of plasmid DNA added to each well was equalized by the addition of empty vector. On the third day, the culture medium was replaced with fresh medium in the presence or absence of 10^{-6} mol/liter forskolin (Sigma-Aldrich Corp., St. Louis, MO). On the fourth day, the cells were lysed in 100 μl/well passive lysis buffer, and the luciferase assay was performed in accordance with the protocol of the Dual-Luciferase Reporter Assay System, using a Lumat LB 9507 luminometer (Berthold Technologies, Bad Wildbad, Germany). The firefly luciferase activity produced by PGL3-ArPII in identically treated triplicate samples was normalized for the renilla luciferase activity produced by phRL-CMV. The data shown are representative of at least three independent experiments.

Living-Cell Laser Confocal Fluorescence Microscopy and FRAP

On the first day, 3×10^5 KGN cells were seeded in 35-mm glass-based dishes (IWAKI, Asahi Techno Glass, Chiba, Japan). On the second day, a total amount of 0.5 μg/dish of various test chimera plasmids was transfected into cells using Superfect. Four hours post transfection, the culture medium was replaced with fresh medium in the presence or absence of 10^{-6} mol/liter forskolin. After overnight incubation (12 h), cells were observed using an LSM 510 META microscope (Carl Zeiss) equipped with a Plan-Apochromat $\times$100 1.4 oil objective.

Transient transfected proteins will potentially cause artifacts from overexpression. Transient transfection also results in a clear cell-to-cell difference of XFP-fusion protein expression level within the same cell population. To roughly overcome these complications, a reference system relating the overexpression level of GFP-X to the endogenous X expression level was established by a quantitative immunofluorescence staining. As a brief example, GFP-DAX-1 is at first transfected to KGN cells, which on the next day was subjected to immunostaining by an anti-DAX-1 antibody and an Alexa Fluor 546-sec antibody. The Alexa Fluor 546 intensity between transfected cells (bearing GFP signal; Alexa Fluor 546 intensity represents both GFP-DAX-1 and endogenous DAX-1), and nontransfected cells (Alexa Fluor 546 intensity represents only endogenous DAX-1) were compared quantitatively and a reference of respective GFP intensity was established. Only cells expressing less than 10-fold [which is usually believed to be near physiological (21)] of endogenous protein level were selected for imaging.

For single fluorescent protein imaging, GFP or YFP fluorescence was excited by the 488-nm or 514-nm laser line, respectively, from an air-cooled fiber-coupled argon laser. For simultaneous imaging of GFP and YFP, a 488-nm laser line was used for excitation, and detection spectrum range was from 491–576 nm. For simultaneous imaging of GFP, YFP, and CFP, a 458-nm laser line was used for excitation, and detection spectrum range was set from 458–587 nm. Raw imagines obtained in a λ-mode were subjected to the META Unmixing procedure to de-mix GFP, YFP, and CFP signals. The reference spectrums for each XFPs were made by imaging cells solely expressing each respective XFP. For GFP, YFP, CFP trilocalization imagining, all three references spectrums were applied for META Unmixing, whereas only GFP and YFP reference spectrums were applied to unmix the GFP and YFP bilocalization images.

Matching the expression levels of proteins being cotransfected is essential to observing a reasonable subcellular interaction. For cotransfection, the amount of each XFP-fusion plasmid was equivalent on a molar basis. During simultaneous multiimaging, cells that express a similar intensity of each fluorescence protein were selected for further study. Parameters such as the laser power, laser line, dichroic beam splitter to separate excitation and emission, scanning speed *etc.*, were all kept fixed during observation of the same group of experimental cells. Colocalization analysis was carried out by LSM software (version 3.0). Line scan analysis was also performed by the software. Fluorescent intensity numerals of each line scan were exported to MS Excel, the mean $\pm$ SD as well as HI values of intensity value for segment of interest were calculated. MS Excel also constructed the line scan fluorescent intensity fluctuation graphs of the representative cells. All images obtained represent the average of eight sequentially obtained images. LSM images were exported as TIF files, and final figures were generated using Adobe Illustrator and Adobe Photoshop (Adobe Systems, Inc., San Jose, CA).

Fluorescence recovery after photobleaching (FRAP) analysis were also carried out by the LSM 510 META confocal microscope. A single Z section was imaged before and at time intervals after a 2-sec bleach. The bleach was carried

out at a wavelength of 514 nm and maximum power for 50 iterations of a box representing 20% of the nuclear volume. A time-interval mode of Time Series was used with the time interval varied in different groups of experiments according to the mobility of the protein: 500 μsec was set for the Ad4BP/SF-1-H89 group (Fig. 8A), 2 sec was for the DAX-1-Ad4BP/SF-1-H89 group (Fig. 8B), and 600 μsec for the DAX-1-Ad4BP/SF-1-FK group (Fig. 8C). The fluorescence intensities of the region of interest were obtained using LSM software (version 3.0), and the data were analyzed using Microsoft Excel. The fluorescence recovery is usually incomplete, probably because attenuation of fluorescence occurs during the serial scanning and also the total amount of fluorescence protein decreases, as around 20% of them have been bleached. In addition, the fluorescent intensity after bleaching is not always the same. Therefore we normalized the raw FRAP data (both intensity of each time point and the time) by the method described by Stenoien *et al.* (51). Briefly, intensity values were normalized using the equation: $It = (Xt - Y)/(Z - Y)$, where I is the intensity at time t, X is the intensity at time t, Y is the intensity immediately after the photobleach (where t is equal to 0), and Z is the intensity at the final time point. This sets the initial postbleach intensity (at $t = 0$ sec) to 0 and the final intensity to 1 using arbitrary units. The normalized intensity values were averaged and plotted against time to make the recovery curve. The $t_{1/2}$ value can be observed from the graph as the time at which the normalized intensity reaches 0.5 arbitrary units. A subgroup of FRAPed cells was traced by initially being seeded on grid-carved glass-bottom dishes (code no. 3920-035, IWAKI, Chiba, Japan), and was subsequently subjected to quantitative immunofluorescence staining to ensure that cells selected for FRAP study also overexpressed both YFP-Ad4BP/SF-1 and pRc/RSV-DAX-1 in a reasonable range as described above.

Statistics

One-way ANOVA followed by Scheffe's test was used for multigroup comparisons.

Acknowledgments

We thank Professor Spiegelman (Department of Cell Biology, Harvard Medical School, Boston, MA) for the generous gift of the expression vector for mouse PGC-1, pcDNA-PGC-1.

Received March 28, 2003. Accepted September 30, 2003.

Address all correspondence and requests for reprints to: Toshihiko Yanase, M.D., Ph.D., Department of Medicine and Bioregulatory Science, Graduate School of Medical Science, Kyushu University, Maidashi 3-1-1, Higashi-ku, Fukuoka 812-8582, Japan. E-mail: yanase@intmed3.med.kyushu-u.ac.jp.

REFERENCES

1. Ingraham HA, Lala DS, Ikeda Y, Luo X, Shen WH, Nachtigal MW, Abbud R, Nilson JH, Parker KL 1994 The nuclear receptor steroidogenic factor 1 acts at multiple levels of the reproductive axis. Genes Dev 8:2302–2312
2. Nawata H, Yanase T, Oba K, Ichino I, Saito M, Goto K, Ikuyama S, Sakai H, Takayanagi R 1999 Human Ad4BP/SF-1 and its related nuclear receptor. J Steroid Biochem Mol Biol 69:323–328
3. Luo X, Ikeda Y, Lala DS, Baity LA, Meade JC, Parker KL 1995 A cell-specific nuclear receptor plays essential roles in adrenal and gonadal development. Endocr Res 21: 517–524
4. Morohashi KI, Omura T 1996 Ad4BP/SF-1, a transcription factor essential for the transcription of steroidogenic cytochrome P450 genes and for the establishment of the reproductive function. FASEB J 10:1569–1577
5. Parker KL, Schimmer BP 1997 Steroidogenic factor 1: a key determinant of endocrine development and function. Endocr Rev 18:361–377
6. Zhao L, Bakke M, Krimkevich Y, Cushman LJ, Parlow AF, Camper SA, Parker KL 2001 Steroidogenic factor 1 (SF1) is essential for pituitary gonadotrope function. Development 128:147–154
7. Luo X, Ikeda Y, Parker KL 1994 A cell-specific nuclear receptor is essential for adrenal and gonadal development and sexual differentiation. Cell 77:481–490
8. Achermann JC, Ito M, Ito M, Hindmarsh PC, Jameson JL 1999 A mutation in the gene encoding steroidogenic factor-1 causes XY sex reversal and adrenal failure in humans. Nat Genet 22:125–126
9. Ikeda Y, Swain A, Weber TJ, Hentges KE, Zanaria E, Lalli E, Tamai KT, Sassone-Corsi P, Lovell-Badge R, Camerino G, Parker KL 1996 Steroidogenic factor 1 and Dax-1 colocalize in multiple cell lineages: potential links in endocrine development. Mol Endocrinol 10:1261–1272
10. Swain A, Zanaria E, Hacker A, Lovell-Badge R, Camerino G 1996 Mouse Dax1 expression is consistent with a role in sex determination as well as in adrenal and hypothalamus function. Nat Genet 12:404–409
11. Crawford PA, Dorn C, Sadovsky Y, Milbrandt J 1998 Nuclear receptor DAX-1 recruits nuclear receptor corepressor N-CoR to steroidogenic factor 1. Mol Cell Biol 18:2949–2956
12. Sewer MB, Nguyen VQ, Huang CJ, Tucker PW, Kagawa N, Waterman MR 2002 Transcriptional activation of human CYP17 in H295R adrenocortical cells depends on complex formation among p54 (nrb)/NonO, protein-associated splicing factor, and SF-1, a complex that also participates in repression of transcription. Endocrinology 143:1280–1290
13. Morohashi K, Zanger UM, Honda S, Hara M, Waterman MR, Omura T 1993 Activation of CYP11A and CYP11B gene promoters by the steroidogenic cell-specific transcription factor, Ad4BP. Mol Endocrinol 7:1196–1204
14. Michael MD, Kilgore MW, Morohashi K, Simpson ER 1995 Ad4BP/SF-1 regulates cyclic AMP-induced transcription from the proximal promoter (PII) of the human aromatase P450 (CYP19) gene in the ovary. J Biol Chem 270:13561–13566
15. Ito M, Park Y, Weck J, Mayo KE, Jameson JL 2000 Synergistic activation of the inhibin α-promoter by steroidogenic factor-1 and cyclic adenosine 3′, 5′-monophosphate. Mol Endocrinol 14:66–81
16. Hager GL, Elbi C, Becker M 2002 Protein dynamics in the nuclear compartment. Curr Opin Genet Dev 12:137–141
17. Stenoien DL, Simeoni S, Sharp ZD, Mancini MA 2000 Subnuclear dynamics and transcription factor function. J Cell Biochem Suppl 35:99–106
18. Becker M, Baumann C, John S, Walker DA, Vigneron M, McNally JG, Hager GL 2002 Dynamic behavior of transcription factors on a natural promoter in living cells. EMBO Rep 3:1188–1194
19. McNally JG, Muller WG, Walker D, Wolford R, Hager GL 2000 The glucocorticoid receptor: rapid exchange with regulatory sites in living cells. Science 287:1262–1265
20. Fletcher TM, Xiao N, Mautino G, Baumann CT, Wolford R, Warren BS, Hager GL 2002 ATP-dependent mobilization of the glucocorticoid receptor during chromatin remodeling. Mol Cell Biol 22:3255–3263
21. Stenoien DL, Patel K, Mancini MG, Dutertre M, Smith CL, O'Malley BW, Mancini MA 2001 FRAP reveals that mobility of oestrogen receptor-α is ligand- and proteasome-dependent. Nat Cell Biol 3:15–23
22. Stenoien DL, Nye AC, Mancini MG, Patel K, Dutertre M, O'Malley BW, Smith CL, Belmont AS, Mancini MA 2001

Ligand-mediated assembly and real-time cellular dynamics of estrogen receptor-coactivator complexes in living cells. Mol Cell Biol 21:4404–4412
23. Maruvada P, Baumann CT, Hager GL, Yen PM 2003 Dynamic shuttling and intranuclear mobility of nuclear hormone receptors. J Biol Chem 278:12425–12432
24. Lynch JP, Lala DS, Peluso JJ, Luo W, Parker KL, White BA 1993 Steroidogenic factor 1, an orphan nuclear receptor, regulates the expression of the rat aromatase gene in gonadal tissues. Mol Endocrinol 7:776–786
25. Saitoh M, Takayanagi R, Goto K, Fukamizu A, Tomura A, Yanase T, Nawata H 2002 The presence of both the amino- and carboxyl-terminal domains in the AR is essential for the completion of a transcriptionally active form with coactivators and intranuclear compartmentalization common to the steroid hormone receptors: a three-dimensional imaging study. Mol Endocrinol 16:694–706
26. Aesoy R, Mellgren G, Morohashi K, Lund J 2002 Activation of cAMP-dependent protein kinase increases the protein level of steroidogenic factor-1. Endocrinology 143:295–303
27. Jacob AL, Lund J, Martinez P, Hedin L 2001 Acetylation of steroidogenic factor 1 protein regulates its transcriptional activity and recruits the coactivator GCN5. J Biol Chem 276:37659–37664
28. McMahon SB, Van Buskirk HA, Dugan KA, Copeland TD, Cole MD 1998 The novel ATM-related protein TRRAP is an essential cofactor for the c-Myc and E2F oncoproteins. Cell 94:363–374
29. Jacq X, Brou C, Lutz Y, Davidson I, Chambon P, Tora L 1994 Human TAFII30 is present in a distinct TFIID complex and is required for transcriptional activation by the estrogen receptor. Cell 79:107–117
30. Yanagisawa J, Kitagawa H, Yanagida M, Wada O, Ogawa S, Nakagomi M, Oishi H, Yamamoto Y, Nagasawa H, McMahon SB, Cole MD, Tora L, Takahashi N, Kato S 2002 Nuclear receptor function requires a TFTC-type histone acetyl transferase complex. Mol Cell 9:553–562
31. Ito M, Yu R, Jameson JL 1997 DAX-1 inhibits SF-1-mediated transactivation via a carboxy-terminal domain that is deleted in adrenal hypoplasia congenita. Mol Cell Biol 17:1476–1483
32. Altincicek B, Tenbaum SP, Dressel U, Thormeyer D, Renkawitz R, Baniahmad A 2000 Interaction of the corepressor Alien with DAX-1 is abrogated by mutations of DAX-1 involved in adrenal hypoplasia congenita. J Biol Chem 275:7662–7667
33. Zhang P, Mellon SH 1996 The orphan nuclear receptor steroidogenic factor-1 regulates the cyclic adenosine 3′, 5′-monophosphate-mediated transcriptional activation of rat cytochrome P450c17 (17α-hydroxylase/c17–20 lyase). Mol Endocrinol 10:147–158
34. Hammer GD, Krylova I, Zhang Y, Darimont BD, Simpson K, Weigel NL, Ingraham HA 1999 Phosphorylation of the nuclear receptor SF-1 modulates cofactor recruitment: integration of hormone signaling in reproduction and stress. Mol Cell 3:521–526
35. Carlone DL, Richards JS 1997 Functional interactions, phosphorylation, and levels of 3′, 5′-cyclic adenosine monophosphate-regulatory element binding protein and steroidogenic factor-1 mediate hormone-regulated and constitutive expression of aromatase in gonadal cells. Mol Endocrinol 11:292–304
36. Sewer MB, Waterman MR 2002 Adrenocorticotropin/cyclic adenosine 3′, 5′-monophosphate-mediated transcription of the human CYP17 gene in the adrenal cortex is dependent on phosphatase activity. Endocrinology 143:1769–1777
37. Nomura M, Kawabe K, Matsushita S, Oka S, Hatano O, Harada N, Nawata H, Morohashi K 1998 Adrenocortical and gonadal expression of the mammalian Ftz-F1 gene encoding Ad4BP/SF-1 is independent of pituitary control. J Biochem (Tokyo) 124:217–224
38. Crawford PA, Sadovsky Y, Woodson K, Lee SL, Milbrandt J 1995 Adrenocortical function and regulation of the steroid 21-hydroxylase gene in NGFI-B-deficient mice. Mol Cell Biol 15:4331–4316
39. Herzig S, Long F, Jhala US, Hedrick S, Quinn R, Bauer A, Rudolph D, Schutz G, Yoon C, Puigserver P, Spiegelman B, Montminy M 2001 CREB regulates hepatic gluconeogenesis through the coactivator PGC-1. Nature 413:179–183
40. Htun H, Barsony J, Renyi I, Gould DL, Hager GL 1996 Visualization of glucocorticoid receptor translocation and intranuclear organization in living cells with a green fluorescent protein chimera. Proc Natl Acad Sci USA 93: 4845–4850
41. Racz A, Barsony J 1999 Hormone-dependent translocation of vitamin D receptors is linked to transactivation. J Biol Chem 274:19352–19360
42. Jenster G 1999 The role of the androgen receptor in the development and progression of prostate cancer. Semin Oncol 26:407–421
43. Fejes-Toth G, Pearce D, Naray-Fejes-Toth A 1998 Subcellular localization of mineralocorticoid receptors in living cells: effects of receptor agonists and antagonists. Proc Natl Acad Sci USA 95:2973–2978
44. Tomura A, Goto K, Morinaga H, Nomura M, Okabe T, Yanase T, Takayanagi R, Nawata H 2001 The subnuclear three-dimensional image analysis of androgen receptor fused to green fluorescence protein. J Biol Chem 276: 28395–28401
45. Elbi C, Misteli T, Hager GL 2002 Recruitment of dioxin receptor to active transcription sites. Mol Biol Cell 13: 2001–2015
46. Baumann CT, Ma H, Wolford R, Reyes JC, Maruvada P, Lim C, Yen PM, Stallcup MR, Hager GL 2001 The glucocorticoid receptor interacting protein 1 (GRIP1) localizes in discrete nuclear foci that associate with ND10 bodies and are enriched in components of the 26S proteasome. Mol Endocrinol 15:485–500
47. Nishi Y, Yanase T, Mu Y, Oba K, Ichino I, Saito M, Nomura M, Mukasa C, Okabe T, Goto K, Takayanagi R, Kashimura Y, Haji M, Nawata H 2001 Establishment and characterization of a steroidogenic human granulosa-like tumor cell line, KGN, that expresses functional follicle-stimulating hormone receptor. Endocrinology 142:437–445
48. Nishi Y, Yanase T, Oba K, Ikuyama S, Takayanagi R, Nawata H 1998 Establishment and function analysis of a steroidogenic human granulosa-like tumor cell line, KGN. Clin Endocrinol (Tokyo) 46:156–161
49. Oba K, Yanase T, Ichino I, Goto K, Takayanagi R, Nawata H 2000 Transcriptional regulation of the human FTZ-F1 gene encoding Ad4BP/SF-1. J Biochem (Tokyo) 128: 517–528
50. Mu YM, Yanase T, Nishi Y, Takayanagi R, Goto K, Nawata H 2001 Combined treatment with specific ligands for PPARγ:RXR nuclear receptor system markedly inhibits the expression of cytochrome P450arom in human granulosa cancer cells. Mol Cell Endocrinol 181:239–248
51. Stenoien DL, Mielke M, Mancini MA 2002 Intranuclear ataxin1 inclusions contain both fast- and slow-exchanging components. Nat Cell Biol 4:806–810

Molecular Endocrinology **is published monthly by The Endocrine Society (http://www.endo-society.org), the foremost professional society serving the endocrine community.**

High-Sensitivity Detection of the A3243G Mutation of Mitochondrial DNA by a Combination of Allele-Specific PCR and Peptide Nucleic Acid-Directed PCR Clamping

Michiyo Urata,[1] Yui Wada,[1] Sang Ho Kim,[1,2] Worawan Chumpia,[1,3] Yuzo Kayamori,[1] Naotaka Hamasaki,[1] and Dongchon Kang[1*]

Background: **The A3243G mutation of mitochondrial DNA (mtDNA) is involved in many common diseases, including diabetes mellitus and mitochondrial encephalomyopathy with lactic acidosis and stroke-like episodes (MELAS). For detection of this mutation, allele-specific PCR is highly sensitive but requires strict control of PCR conditions; it thus is not adequate for a routine clinical test. We aimed to develop a routinely available PCR method for quantitative detection of low-level heteroplasmy of the A3243G mutation.**

Methods: **Quantitative allele-specific PCR for the A3243G mutation was performed in the presence of peptide nucleic acid (PNA), in which PNA is complementary to the wild-type mtDNA, with one primer having a 3′ end matched to nucleotide position 3243 of the mutant.**

Results: **With our method, amplification of wild-type mtDNA was suppressed 7000-fold compared with amplification of the mutant mtDNA under a broad range of conditions: DNA, 5–100 ng; annealing temperature, 61–66 °C; and PNA, 1.5–3.5 μmol/L. Hence, 0.1% heteroplasmy of the A3243G mutation can be reliably quantified by this method. Blood samples form 40 healthy volunteers showed <0.06% heteroplasmy, suggesting that 0.1% is diagnostically significant.**

Conclusions: **PNA maintains the specificity of allele-specific PCR over a wide range of conditions, which is important for routine clinical testing.**

All vertebrate mitochondria have semi-autonomously replicating extranuclear genomes. Human mitochondrial DNA (mtDNA)[4] encodes 13 subunits of the mitochondrial respiratory chain, 22 tRNAs, and 2 rRNAs, all of which are essential for assembly of the mitochondrial respiratory chain that produces most of the cellular ATP. Inherited mtDNA mutations have been associated with a variety of neuromuscular disorders *(1)*. More than 100 different mtDNA mutations have been reported to be related to various disorders, and that number is still increasing *(1)*. Because a cell may contain hundreds to thousands of mtDNA molecules, heteroplasmy (coexistence of wild-type and mutant mtDNA in a single cell) is usually present in mitochondrial diseases. Disease symptoms appear only when the percentage of mutant mtDNA exceeds a particular value (threshold). It is therefore common to find that affected tissues show a high percentage of the specific heteroplasmy, whereas other, apparently unaffected cells in the same individual have much lower percentages of the heteroplasmy or show no detectable mutations at that site.

Mitochondrial mutations are broadly classified into two groups: rearrangements (deletions and duplications) and point mutations. Among point mutations, an A-to-G

[1] Department of Clinical Chemistry and Laboratory Medicine, Kyushu University, Graduate School of Medical Sciences, Fukuoka, Japan.

[2] Department of Biology Education, Daegue University, Kyungsan, Korea.

[3] Thalassemia Research Center, Institute of Science and Technology for Research and Development, Mahidol University, Nakornpathom, Thailand.

*Address correspondence to this author at: Department of Clinical Chemistry and Laboratory Medicine, Kyushu University Graduate School of Medical Sciences, 3-1-1 Maidashi Higashi-ku, Fukuoka 812-8582, Japan. Fax 81-92-642-5772; e-mail kang@mailserver.med.kyushu-u.ac.jp.

Received March 4, 2004; accepted August 19, 2004.

Previously published online at DOI: 10.1373/clinchem.2004.033761

[4] Nonstandard abbreviations: mtDNA, mitochondrial DNA; np, nucleotide position; MELAS, mitochondrial encephalomyopathy with lactic acidosis and stroke-like episodes; DM, diabetes mellitus; RFLP, restriction fragment length polymorphism; LMPCR, ligation-mediated PCR; PNA, peptide nucleic acid; T_m, melting temperature; and SNP, single-nucleotide polymorphism.

mutation at nucleotide position (np) 3243 in the human mitochondrial $tRNA^{Leu}$(UUR) gene (A3243G) is the most common. This particular mutation accounts for ~80% of patients with mitochondrial encephalomyopathy with lactic acidosis and stroke-like episodes (MELAS) *(2, 3)*. The percentage of cells containing mtDNA with the heteroplasmic A3243G mutation varies from tissue to tissue as described above and may be highest in affected tissues such as muscle and brain. However, samples that may be easily attained in a noninvasive manner and routinely used, such as blood or urinary cells, usually show lower percentages of heteroplasmy. For example, the A3243G mutation was detected in the blood of only 5 of 10 patients but was detected in the muscle of all 10 patients *(4)*.

In addition to the classic mitochondrial encephalomyopathies such as MELAS, the A3243G mtDNA mutation has been shown to be involved type II diabetes mellitus (DM) and aging *(5)*. Normal ATP production in mitochondria is critical, particularly for insulin secretion from pancreatic beta cells *(6)*. Consistent with this fact, individuals with various types of MELAS often have symptoms of diabetes *(7, 8)*, and accumulation of the mutation in pancreatic beta cells could cause adult-onset DM. In fact, the mutation is also found in patients with DM who were not previously diagnosed with MELAS *(9)*. Although many of these patients exhibit a variety of neurologic disorders, typically including deafness, the A3243G mutation has also been found in DM patients with few neuromuscular symptoms. Considering that the heteroplasmy may be highest in affected tissues, the pancreas may be a good source for examination of the A3243G mutation in patients with diabetes *(10)*; however, pancreatic biopsy is not available for routine screening. Instead, peripheral leukocytes and urinary epithelial cells, which are obtained in a noninvasive manner, are commonly used in screening. The percentage of mtDNA mutations is usually higher in the latter than in the former *(11–13)*.

The A3243G mutation creates a new restriction site for the restriction enzyme *ApaI*; thus, this mutation is typically surveyed by a conventional PCR-restriction fragment length polymorphism (RFLP) method in which a region including np 3243 is PCR-amplified, digested with *ApaI*, and then stained with ethidium bromide after agarose gel electrophoresis. This method can barely detect the heteroplasmy at concentrations of 5–10% *(14)*. Although the prevalence of DM patients with the A3243G mutation is estimated to be 1–2% of all DM patients *(8)*, it is highly likely that the A3243G mutation will be missed in some DM patients by the RFLP method using peripheral blood cells *(14, 15)*. To address this issue, we previously developed a sensitive ligation-mediated PCR-based (LMPCR) method that is able to detect the A3243G heteroplasmy present at a concentration of 0.01% *(16)*. With the LMPCR method, we were able to detect the heteroplasmy present at 0.01–0.1% in approximately one-half of 136 apparently healthy volunteers; no volunteer had more than 0.1%. On the other hand, we found that the heteroplasmy was present in concentrations >0.1% in the leukocytes of 1% of 233 patients with type II DM.

This LMPCR method is very specific and highly sensitive, but it is only semiquantitative, in addition to being somewhat laborious and time-consuming. Thus, it is not an ideal routine clinical test, especially for large numbers of samples. We developed a sensitive quantitative method that combines peptide nucleic acid (PNA) and allele-specific PCR (Fig. 1, bottom panel). This combination increases the detection of the A3243 heteroplasmy by approximately two orders of magnitude more than use of PNA-directed PCR-clamping alone (Fig. 1, top panel).

Materials and Methods

BLOOD DONORS AND CELL LINES

Blood from 40 healthy donors who were mainly workers in the Kyushu University Hospital was collected in tubes containing 1.5 g/L disodium EDTA. The donors ranged in age from their twenties to their fifties [mean (SD) age, 38.7 (11.9) years] and included five males and five females in each 10-year age group. Blood sampling was performed after receipt of informed consent according to the ethics guidelines of the Kyushu University Hospital. Two cybrid

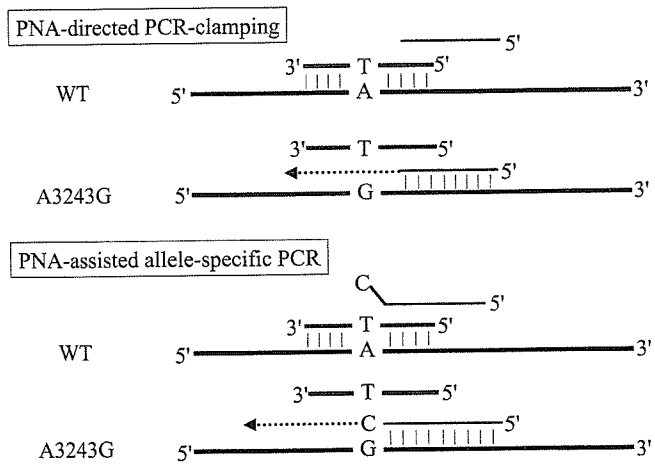

Fig. 1. Schemes for PNA-directed PCR clamping and PNA-assisted allele-specific PCR.

The L-strand of mtDNA around 3243 is shown as a *thick black line*. The 3243 site is shown only by a nucleotide. *Thin black* and *thick gray lines* indicate a DNA primer and PNA, respectively. The *dotted arrow* denotes newly synthesized DNA. The PNA is designed to completely match a wild-type (*WT*) mtDNA region including np 3243 at its middle. In PNA-directed PCR-clamping (*top panel*), an antisense primer DNA is designed to partly overlap the PNA-binding region but not to reach np 3243. PNA usually binds to a DNA strand more strongly than does naturally occurring DNA; therefore, the PNA expels the 3′ side of the primer from wild-type mtDNA and inhibits the amplification of wild-type mtDNA. In general, one nucleotide mismatch makes the binding of PNA much weaker. Therefore, the primer instead of the PNA binds to 3243 mutant mtDNA, leading to amplification of the mutant mtDNA. In PNA-assisted allele-specific PCR (*bottom panel*), an antisense primer is designed to end at np 3243 and to match to the 3243 mutant. Because of this 3′ mismatch, the amplification of wild-type mtDNA is largely suppressed. In addition, because the PNA expels the 3′ side of the primer, the amplification of wild-type mtDNA is further inhibited. The PNA is more efficiently detached from the 3243 mutant mtDNA in PNA-assisted allele-specific PCR than in PNA-directed PCR clamping because the primer overlaps the PNA region longer in the former than in the latter.

cell lines carrying 100% wild-type and 100% A3243G mutant mtDNA (2SA and 2SD, respectively) were made by fusion of human mtDNA-deficient rho^0 206 cells and enucleated fibroblasts derived from a patient with A3243G MELAS *(17)*.

PREPARATION OF DNA

The total DNA of the cell lines and peripheral leukocytes was extracted with QIAamp DNA extraction reagents (QIAGEN). The DNA was treated with RNase A, extracted with phenol–chloroform (1:1 by volume), precipitated with ethanol, resolubilized in 20 μL of distilled water, and quantified based on the absorbance at 260 nm.

PNA-ASSISTED ALLELE-SPECIFIC PCR

PNA (5′-ACCGGGCTCTGCCAT-3′), which was designed to bind the L-strand, was obtained from FASMAC Co., Ltd. A sense primer, mtL1-1 (5′-CAT AAC ACA GCA AGA CGA GAA GAC CCT ATG G-3′), and an antisense primer, mt3243HC (5′-TTT TAT GCG ATT ACC GGG CC-3′), were used. The standard PCR reaction mixture consisted of 1× LightCycler mixture (LC-FastStart Reaction Mix SYBR GREEN I; Roche) containing the DNA-binding fluorescent dye SYBR Green I and *Taq* DNA polymerase, 2.5 μM PNA, 0.25 μM each primer, and 10 ng of total DNA in 20 μL. Thermal cycling was conducted in a LightCycler. The standard conditions were as follows: an initial DNA denaturation step of 10 min at 94 °C and an amplification step of 20 s at 94 °C, 5 s at 77 °C, 5 s at 70 °C, 10 s at 64 °C, and 20 s at 72 °C. The 5 s at 77 °C and 5 s at 70 °C steps were inserted to slow the temperature decrease and allow binding of PNA to DNA. DNA amplification was monitored in real time.

QUANTIFICATION OF mtDNA

An ~300-bp DNA fragment (np 16052–16361) was PCR-amplified with sense primer 5mt16052 (5′-CCA CCC AAG TAT TGA CTC ACC C-3′) and antisense primer 3mt339 (5′-CGA GAA GGG ATT TGA CTG TAA TG-3′). The PCR product was cloned into a TA vector, pQTmt. The plasmid was quantified by the absorbance at 260 nm and used as the calibrator for total mtDNA (wild-type and the A3243G mutant) quantification. The PCR reaction mixture for the quantification consisted of 1× LightCycler mixture, 2.0 mM $MgCl_2$, 0.5 μM each primer, and various amounts of the pQTmt plasmid in 20 μL. Thermal cycling was conducted in a LightCycler. The standard thermocycling conditions were as follows: an initial DNA denaturation step of 10 min at 95 °C and an amplification step of 15 s at 95 °C, 5 s at 60 °C, and 15 s at 72 °C.

Similarly, an ~560-bp DNA fragment including the A3243G mutation (np 2703–3262) was PCR-amplified with mtL1-1 and antisense primer mt3243HC (the same as for the allele-specific PCR) and cloned into a TA vector; we named this plasmid pQMmt and used it as the calibrator for the A3243G mutant.

Results and Discussion

DETERMINATION OF PCR CONDITIONS

We determined the optimum conditions for amplification of the A3243G mutant mtDNA in two human cell lines, 2SA and 2SD, which carry 100% wild-type and 100% A3243G mutant mtDNA, respectively. The two cell lines contained essentially the same copy number of mtDNA per total DNA (see the "Total" column in Table 1). When we performed allele-specific PCR in the presence of PNA using 10 ng of total DNA in 20 μL of the reaction mixture, the crossing point of 2SD was ~15 cycles earlier than that of 2SA (Fig. 2A). The final fluorescent intensity of SYBR Green I, which indicates the amount of double-stranded DNA, was ~30% lower in 2SA than in 2SD. We mixed the two total DNAs at various ratios (from 0.1% to 10% 2SD) and found that 2SA DNA with 0.1% 2SD added could be clearly distinguished from 100% 2SA (Fig. 2A). By constructing a calibration curve of crossing points vs percentage of 2SD (100% to 0.1%; Fig. 2B), we could estimate a 2SA concentration that corresponded to a mean (SD) of 0.014 (0.0008)% of 2SD (n = 3). Given that 2SA is 100% wild type, the amplification of wild-type mtDNA was apparently suppressed ~7000-fold compared with the A3243G mutant in this PNA-assisted allele-specific PCR. The PCR products at the endpoint of the reaction (i.e., after 50 cycles) are shown in Fig. 2C.

The PCR products for 2SD were found at their anticipated band length of ~560 bp (Fig. 2C, lane 1). However, in the case of 2SA, the 560-bp product was much less prominent, and a lower band that may be derived from the presence of "primer-dimers" was detected (Fig. 2C, lane 5). The lower band was also observed in the absence of mtDNA (Fig. 2C, lane 6). Notably, the lower primer-dimer band was hardly seen even in 0.1% 2SD (Fig. 2C, lane 4), suggesting that the primer-dimer is formed only when the amount of the mutant 3243 mtDNA is extremely low or absent. From these results, the erroneous amplification of wild-type mtDNA may actually be much lower than that estimated by the fluorescence. As shown in the melting curves of the PCR products (Fig. 2D), the 560-bp product and the primer-dimer were readily distin-

Table 1. Estimation of 3243 heteroplasmy.[a]

	Mean (SD) mtDNA copy number/ng total DNA		
	Total	Mutant	Heteroplasmy, %
100% 2SD	19.1 (1.4) × 10^4	18.6 (3.4) × 10^4	97.3 (10.4)
10% 2SD	17.5 (1.6) × 10^4	1.7 (0.5) × 10^4	9.7 (1.7)
100% 2SA	18.6 (1.6) × 10^4	31.3 (11.6)	0.013 (0.005)

[a] Conditions were as follows: 2.5 μM PNA, 10 ng of total DNA, and an annealing temperature of 64 °C. The copy numbers of total mtDNA and mutant mtDNA were measured as described in the *Materials and Methods*. Three independent experiments were performed, with each experiment containing three measuring points. The means in each experiment were averaged, and the result is presented as the mean (SD). The heteroplasmy was determined by mean values of total and mutant copy numbers in each independent experiment, and then those values were averaged.

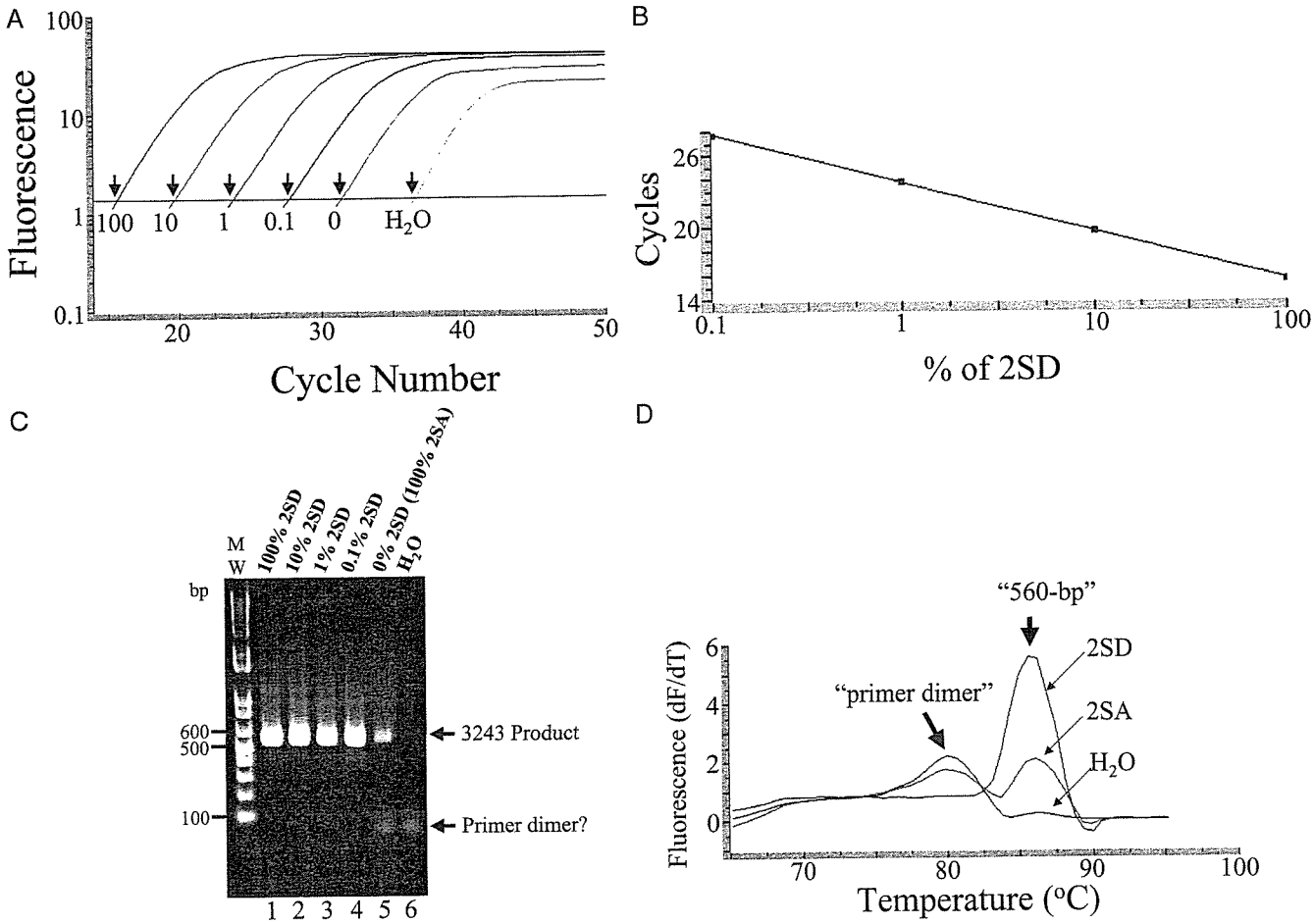

Fig. 2. Amplification of mtDNA carrying A3243G.

(*A*), total DNA from 2SD (100% mutant) and 2SA (100% wild type) cells was mixed and used for quantitative PCR of mtDNA carrying A3243G. The combined amount of DNA was 10 ng in the reaction mixture. The PNA concentration was 2.5 μM, and the annealing temperature was 64 °C. Each value *below* the *horizontal line* indicates the percentage of 2SD DNA, such that 0 (zero) indicates 100% 2SA. *H_2O* indicates that the PCR was done in the absence of DNA. *Arrows* indicate crossing points. (*B*), calibration curve for the crossing points against percentage of 2SD. (*C*), PCR products after 50 cycles were electrophoresed on a 1.0% agarose gel and stained with ethidium bromide. *Lane MW*, molecular markers. (*D*), melting curves of PCR products after 50 cycles. The fluorescence of PCR products is differentiated on the *y axis* (dF/dT) with respect to temperature. H_2O and 2SD showed a peak at 80 and 86 °C, respectively, whereas 2SA showed peaks at both of these temperatures.

guished, with the former having a higher melting temperature (T_m) than the latter (Fig. 2D).

We also examined whether this 15-cycle difference is maintained at different concentrations of total DNA. We varied the DNA amount from 1 to 100 ng. The 15-cycle difference was maintained between 5 and 100 ng (see Table 1 in the Data Supplement that accompanies the online version of this article at http://www.clinchem.org/content/vol50/issue11/). In addition, we changed the annealing temperatures from 60 °C to 68 °C. The 15-cycle difference was not affected much between 61 and 66 °C (Table 2 in the online Data Supplement). It is striking that the allele-specific PCR allows such a broad range of annealing temperatures because usually strict control of annealing temperatures is critical for assuring high specificity, particularly in cases with heteroplasmy <1%. Finally, we examined the effect of the PNA concentration. Without PNA, allele-specific PCR revealed an ~10-cycle difference between 2SA and 2SD, whereas the presence of PNA increased the difference by ~5 cycles (Table 3 in the online Data Supplement). These results suggest that allele-specific PCR plus PNA increases the specificity of amplification of the A3243G mutant by two orders of magnitude more than does PNA alone. The 15-cycle difference was observed with PNA concentrations between 1.5 and 3.5 μmol/L (Table 3 in the online Data Supplement).

DETERMINATION OF mtDNA COPY NUMBER

To quantitatively estimate the heteroplasmy, we determined the copy numbers of the mutant and total mtDNA. For the former, plasmid pQMmt, which includes a DNA fragment (np 2703–3262) containing the A3243G mutation was constructed and used as the copy number calibrator for the mutant mtDNA. We also added PNA in the PCR reaction mixtures for the calibration curve to adjust the

amplification efficiency of the mutant mtDNA. For the latter, plasmid pQTmt, which includes a DNA fragment (np 16052–16361), was constructed and used as the calibrator for determining copy number. Using these two plasmids, we measured the copy numbers of mutant and total mtDNA in 2SA and 2SD cells and then calculated the heteroplasmy. The heteroplasmy of 2SD cells was 97.3%, which is close to 100% (Table 1). The value for 2SA (0.013%) is consistent with the estimate that was obtained by mixing 2SA and 2SD (Fig. 2) and suggests that ~0.02% heteroplasmy is a background in this measurement system. The mixture of 2SA and 2SD DNA exhibited amounts of heteroplasmy close to the mixing ratio (Table 1).

We next measured the heteroplasmy in blood samples from 40 apparently healthy volunteers. When examining the specimens from the volunteers, we always measured 2SD in parallel. The obtained heteroplasmy value of the 2SD sample was divided by a factor and adjusted to 100%. For example, when the assay found 95% heteroplasmy for 2SD from the measured copy numbers of mutant and wild-type mtDNA, we divided the 95% by a factor of 0.95, and the same factor was applied to the values for the specimens to minimize measurement errors. When we used these techniques, no volunteer had more than 0.06% heteroplasmy [mean (SD), 0.03 (0.01)%]. We therefore concluded that finding 0.1% heteroplasmy is a reliable indication of the presence of the mutation.

We then tested this method with two MELAS patients, P1 and P2 (80% and 20% heteroplasmy, respectively, according to our method; Fig. 3A). The results of conventional PCR-RFLP analysis of those samples are shown in Fig. 3B. The results for patient P2 were markedly different from those for 2SA in the PNA-assisted allele-specific PCR assay (Fig. 3A), but the *Apa*I-cleaved bands in the sample from patient P2 were only weakly visible in the PCR-RFLP gel (Fig. 3B). The DNA from patient P1 was diluted 8-, 80-, and 800-fold with DNA of a healthy individual to make 10%, 1%, and 0.1% heteroplasmy, and the resulting theoretical 0.1% heteroplasmy was clearly distinguished from the DNA of a healthy volunteer (Fig. 3C). These results suggest that this new method is similarly sensitive for DNA extracted from peripheral blood cells from MELAS patients. We also examined 50 patients

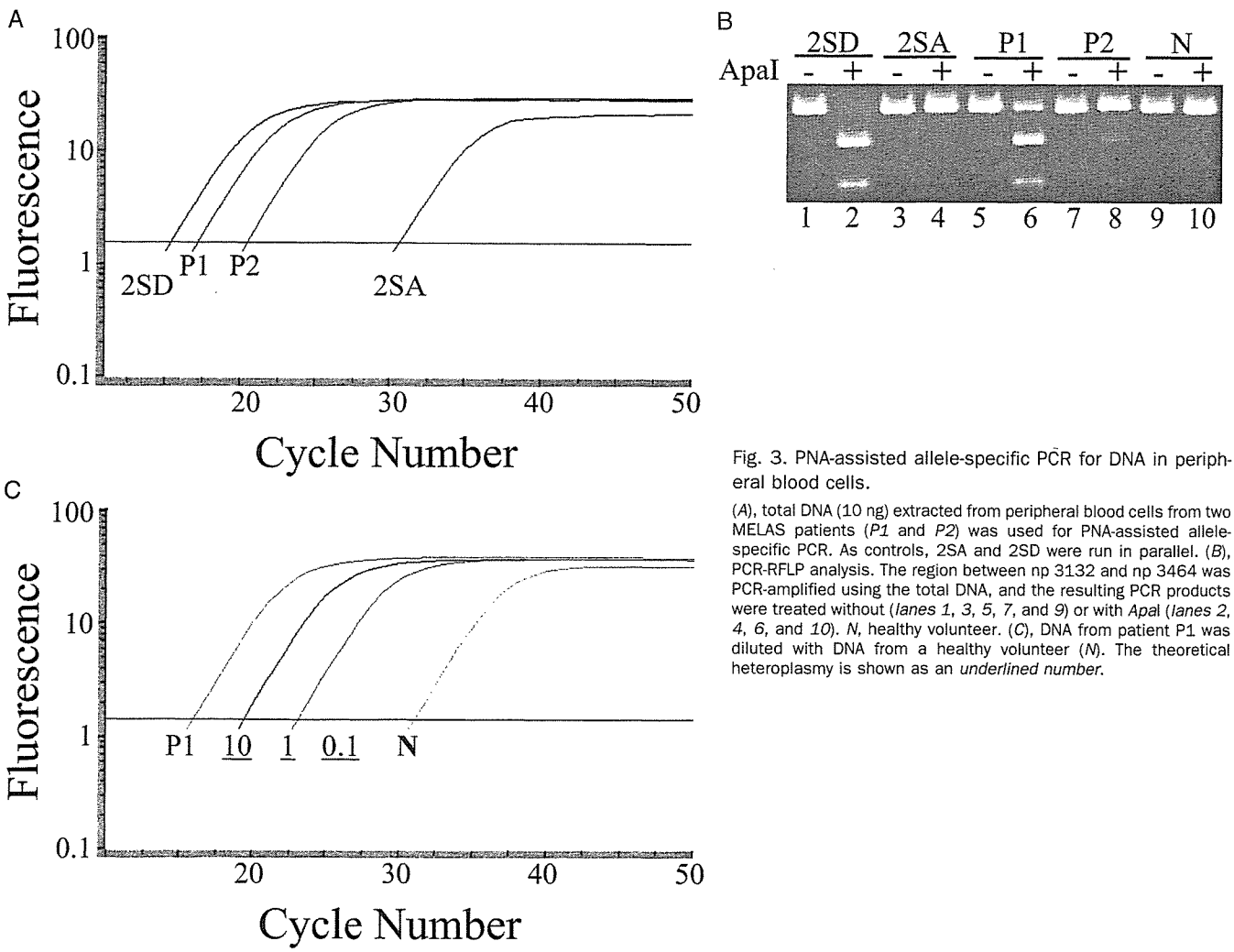

Fig. 3. PNA-assisted allele-specific PCR for DNA in peripheral blood cells.

(*A*), total DNA (10 ng) extracted from peripheral blood cells from two MELAS patients (*P1* and *P2*) was used for PNA-assisted allele-specific PCR. As controls, 2SA and 2SD were run in parallel. (*B*), PCR-RFLP analysis. The region between np 3132 and np 3464 was PCR-amplified using the total DNA, and the resulting PCR products were treated without (*lanes 1, 3, 5, 7,* and *9*) or with *Apa*I (*lanes 2, 4, 6,* and *10*). *N*, healthy volunteer. (*C*), DNA from patient P1 was diluted with DNA from a healthy volunteer (*N*). The theoretical heteroplasmy is shown as an *underlined number.*

with type II DM and found 2 positive individuals, with 20% and 40% heteroplasmy, respectively (results not shown).

Murdock et al. *(18)* have reported that 0.1% heteroplasmy of the A3243G mutation is detected by a PNA-directed PCR-clamping method. However, in their report, the PCR product for the mutation was barely detectable at a 1% concentration when wild-type and mutant DNA were mixed at 100:1. Thus, they needed to perform a second round of PCR to make the signals visible. In addition, digestion of the second-round PCR products with a restriction enzyme was required to confirm the presence of the mutation because wild-type mtDNA was significantly amplified even at 1% in their system. Hancock et al. *(19)* also reported detection of 0.1% heteroplasmy by PNA-directed PCR clamping. Similarly, they needed to sequence the PCR products to confirm the A3243G mutation and to ensure that no other mutation interfered with the PNA binding to the wild type. Initially, we also attempted simple PNA-directed PCR clamping under many conditions, but we never succeeded in completely selectively amplifying the mutant mtDNA, even at 1%; i.e., wild-type mtDNA was always significantly amplified. Thus, under the present conditions, it seems to be impossible to completely suppress the amplification of wild-type mtDNA with PNA alone when the heteroplasmy is 1% and the wild type is 99%. An advantage to using a primer that does not overlap the 3243 site (Fig. 1, top panel) is that amplification of the mutant mtDNA can be definitively confirmed by enzyme digestion or sequencing *(18, 19)*. However, in our PNA-assisted allele-specific PCR (Fig. 1, bottom panel), we did not take this approach because we wished to develop a simple but quantitative method that can be performed in a typical clinical laboratory. Our method provides high specificity over a broad range of PCR conditions. Especially striking is that selective amplification is maintained over a wide range of annealing temperatures. This is particularly important from the point of view of routine clinical tests because we frequently encounter the problem of undesirable amplification by allele-specific PCR as a result of small fluctuations in the annealing temperature in PCR instruments, particularly when we are trying to detect very low percentages of heteroplasmy. We believe that the simple addition of PNA to any allele-specific PCR may generally improve the stability of allele-specific amplification.

The T_m of PNA/DNA is usually reduced by one base mismatch much more than is that of wild-type DNA/DNA. The PNA-directed PCR clamping is strongly based on this principle. However, this strong dependence on base matching could create an adverse situation if there is single-nucleotide polymorphism (SNP) in the region of PNA clamping, such that the wild-type genome is falsely amplified. This is also true for our PNA-assisted allele-specific PCR, although it is not totally dependent on the T_m of PNA. Fortunately, we did not find any SNPs from np 3236 to np 3250, the clamping region of our PNA, in the databases of Ingman et al. (76 persons) *(20)*, Finnila et al. (192 persons) *(21)*, Kong et al. (48 persons) *(22)*, or Herrnstadt et al. (560 persons) *(23)*. No SNPs in this region are found in the Japanese database for ~1000 Japanese *(24)* or in the US database *(1)*. Thus, this region is well conserved, and SNPs in the region may be extremely rare. Two cases with Kearns–Sayre syndrome are reported to harbor mutations at 3249 and 3250, respectively *(1)*. For these cases, a false positive may be better than a false negative. A patient who has a false-positive result for A3243G would then receive further examination for confirmation.

In conclusion, we show that 0.1% heteroplasmy is reliably and quantitatively detected by PNA-assisted allele-specific PCR and that the value 0.1% is not simply the lower limit of detection. When we previously measured heteroplasmy by LMPCR, we detected 0.01% heteroplasmy in peripheral blood cells from approximately one half of the healthy individuals and DM patients, but no healthy individuals had >0.1% heteroplasmy *(16)*. This observation was confirmed by the method presented in this report. Murdock et al. *(18)* also reported that the A3243G mutation does not typically accumulate above 0.1% with age, even in muscle or brain. Therefore, the presence of heteroplasmy >0.1% may be diagnostically significant. It is well established that healthy people typically harbor very low concentrations of the A3243G heteroplasmy *(18, 25)*. Recently, the authors of a case study reported that the concentration of the 3243 mutation in peripheral blood cells of a patient with mitochondrial diabetes was 0.102% *(26)*. Thus, the quantitative detection of 0.1% heteroplasmy appears to be a required and sufficient prerequisite for a practical clinical test for the A3243G mutation. Our method feasibly satisfies this condition and thus may be suitable for a routine clinical test. Because collecting urine samples is less invasive than collecting blood and the concentration of mtDNA mutations is usually much higher in urine samples than in blood samples *(11–13)*, application of this method to urine samples may be even more useful as a routine clinical test.

We extend special thanks to an anonymous reviewer for kind and extensive editing of the manuscript. This work was supported in part by the Uehara Memorial Foundation, the Naito Foundation, and Grants-in-Aid for Scientific Research from the Ministry of Education, Science, Technology, Sports, and Culture of Japan.

References

1. Wallace DC, Lott MT. MITOMAP: a human mitochondrial genome database. http://www.mitomap.org (accessed May 2004).
2. Liang MH, Wong LJ. Yield of mtDNA mutation analysis in 2,000 patients. Am J Med Genet 1998;77:395–400.

3. Wong LJ, Senadheera D. Direct detection of multiple point mutations in mitochondrial DNA. Clin Chem 1997;43:1857–61.
4. Sue CM, Quigley A, Katsabanis S, Kapsa R, Crimmins DS, Byrne E, et al. Detection of MELAS A3243G point mutation in muscle, blood and hair follicles. J Neurol Sci 1998;161:36–9.
5. Kang D, Hamasaki N. Mitochondrial oxidative stress and mitochondrial DNA. Clin Chem Lab Med 2003;41:1281–8.
6. Wollheim CB. Beta-cell mitochondria in the regulation of insulin secretion: a new culprit in type II diabetes. Diabetologia 2000;43: 265–77.
7. Rotig A, Bonnefont J-P, Munnich A. Mitochondrial diabetes mellitus. Diabetes Metab 1996;22:291–8.
8. Gerbitz K-D, van den Ouweland JMW, Maassen JA, Jaksch M. Mitochondrial diabetes: a review. Biochim Biophys Acta 1995; 1271:253–60.
9. Kadowaki T, Kadowaki H, Mori Y, Tobe K, Sakuta R, Suzuki Y, et al. A subtype of diabetes mellitus associated with a mutation of mitochondrial DNA. N Engl J Med 1994;330:962–8.
10. Kobayashi T, Nakanishi K, Nakase H, Kajio H, Okubo M, Murase T, et al. In situ characterization of islets in diabetes with a mitochondrial DNA mutation at nucleotide position 3243. Diabetes 1997;46:1567–71.
11. Hotta O, Inoue CN, Miyabayashi S, Furuta T, Takeuchi A, Taguma Y. Clinical and pathologic features of focal segmental glomerulosclerosis with mitochondrial tRNALeu(UUR) gene mutation. Kidney Int 2001;59:1236–43.
12. Nishigaki Y, Tadesse S, Bonilla E, Shungu D, Hersh S, Keats BJ, et al. A novel mitochondrial tRNA(Leu(UUR)) mutation in a patient with features of MERRF and Kearns-Sayre syndrome. Neuromuscul Disord 2003;13:334–40.
13. Puomila A, Viitanen T, Savontaus ML, Nikoskelainen E, Huoponen K. Segregation of the ND4/11778 and the ND1/3460 mutations in four heteroplasmic LHON families. J Neurol Sci 2002;205: 41–5.
14. Smith ML, Hua X-Y, Marsden DL, Liu D, Kennaway NG, Ngo K-Y, et al. Diabetes and mitochondrial encephalomyopathy with lactic acidosis and stroke-like episodes (MELAS): radiolabeled polymerase chain reaction is necessary for accurate detection of low percentages of mutation. J Clin Endocrinol Metab 1997;82: 2816–31.
15. Suzuki Y, Goto Y, Taniyama M, Nonaka I, Murakami N, Hosokawa K, et al. Muscle histopathology in diabetes mellitus associated with mitochondrial tRNALeu(UUR) mutation at position 3243. J Neurol Sci 1997;145:49–53.
16. Urata M, Wakiyama M, Iwase M, Yoneda M, Kinoshita S, Hamasaki N, et al. New sensitive method for the detection of the A3243G mutation of human mitochondrial deoxyribonucleic acid in diabetes mellitus patients by ligation-mediated polymerase chain reaction. Clin Chem 1998;44:2088–93.
17. Yoneda M, Miyatake T, Attardi G. Complementation of mutant and wild-type human mitochondrial DNAs coexisting since the mutation event and lack of complementation of DNAs introduced separately into a cell within distinct organelles. Mol Cell Biol 1994;14:2699–712.
18. Murdock DG, Christacos NC, Wallace DC. The age-related accumulation of a mitochondrial DNA control region mutation in muscle, but not brain, detected by a sensitive PNA-directed PCR clamping based method. Nucleic Acids Res 2000;28:4350–5.
19. Hancock DK, Schwarz FP, Song F, Wong LJ, Levin BC. Design and use of a peptide nucleic acid for detection of the heteroplasmic low-frequency mitochondrial encephalomyopathy, lactic acidosis, and stroke-like episodes (MELAS) mutation in human mitochondrial DNA. Clin Chem 2002;48:2155–63.
20. Ingman M, Kaessmann H, Paabo S, Gyllenstein V. Mitochondrial genome variation and the origin of modern humans. Nature 2000;408:708–13.
21. Finnila S, Lehtonen MS, Majamaa K. Phylogenetic network for European mtDNA. Am J Hum Genet 2001;68:1475–84.
22. Kong QP, Yao YG, Sun C, Bandelt HJ, Zhu CL, Zhang YP. Phylogeny of east Asian mitochondrial DNA lineages inferred from complete sequences. Am J Hum Genet 2003;73:671–6.
23. Herrnstadt C, Elson JL, Fahy E, Preston G, Turnbull DM, Anderson C, et al. Reduced-median-network analysis of complete mitochondrial DNA coding-region sequences for the major African, Asian, and European haplogroups. Am J Hum Genet 2002;70:1152–71.
24. Tanaka M. Human mitochondrial genome polymorphism database. http://www.giib.or.jp/mtsnp/index_e.html (accessed May 2004).
25. Nomiyama T, Tanaka Y, Hattori N, Nishimaki K, Nagasaka K, Kawamori R, et al. Accumulation of somatic mutation in mitochondrial DNA extracted from peripheral blood cells in diabetic patients. Diabetologia 2002;45:1577–83.
26. Suzuki Y, Nishimaki K, Taniyama M, Muramatsu T, Atsumi Y, Matsuoka K, et al. Lipoma and opthalmoplegia in mitochondrial diabetes associated with small heteroplasmy level of 3243 tRNA(Leu(UUR)) mutation. Diabetes Res Clin Pract 2004;63: 225–9.

Architectural Role of Mitochondrial Transcription Factor A in Maintenance of Human Mitochondrial DNA

Tomotake Kanki,[1] Kippei Ohgaki,[1] Martina Gaspari,[2] Claes M. Gustafsson,[2] Atsushi Fukuoh,[1] Narie Sasaki,[3] Naotaka Hamasaki,[1] and Dongchon Kang[1]*

Department of Clinical Chemistry and Laboratory Medicine, Kyushu University Graduate School of Medical Sciences, Higashi-ku, Fukuoka,[1] and Department of Biology, Faculty of Science, Ochanomizu University, Tokyo,[3] Japan, and Department of Medical Nutrition, Karolinska Institute, Novum, Hudddinge, Sweden[2]

Received 29 December 2003/Returned for modification 17 March 2004/Accepted 26 August 2004

Mitochondrial transcription factor A (TFAM), a transcription factor for mitochondrial DNA (mtDNA) that also possesses the property of nonspecific DNA binding, is essential for maintenance of mtDNA. To clarify the role of TFAM, we repressed the expression of endogenous TFAM in HeLa cells by RNA interference. The amount of TFAM decreased maximally to about 15% of the normal level at day 3 after RNA interference and then recovered gradually. The amount of mtDNA changed closely in parallel with the daily change in TFAM while in organello transcription of mtDNA at day 3 was maintained at about 50% of the normal level. TFAM lacking its C-terminal 25 amino acids (TFAM-ΔC) marginally activated transcription in vitro. When TFAM-ΔC was expressed at levels comparable to those of endogenous TFAM in HeLa cells, mtDNA increased twofold, suggesting that TFAM-ΔC is as competent in maintaining mtDNA as endogenous TFAM under these conditions. The in organello transcription of TFAM-ΔC-expressing cells was no more than that in the control. Thus, the mtDNA amount is finely correlated with the amount of TFAM but not with the transcription level. We discuss an architectural role for TFAM in the maintenance of mtDNA in addition to its role in transcription activation.

Human mitochondrial DNA (mtDNA) is a 16.5-kb double-stranded circular molecule that encodes 13 essential protein components of the mitochondrial oxidative phosphorylation complexes. The maintenance of mtDNA integrity is essential for normal function of the respiratory chain that is responsible for aerobic ATP production. There are hundreds to thousands of copies of mtDNA in one cell. Because the level of mtDNA transcripts largely depends on the copy number of mtDNA, the regulation of its copy number is important for maintaining mitochondrial ATP production. However, the regulation of mtDNA copy number is still poorly understood.

Mitochondrial transcription factor A (TFAM) (11, 30), a transcription factor for mtDNA, enhances mtDNA transcription in a promoter-specific fashion in the presence of mitochondrial RNA polymerase and transcription factor B (TFB1 M or TFB2 M) (10, 23). TFAM is a member of the high-mobility group (HMG) proteins because it contains two HMG boxes. TFAM possesses DNA-binding properties regardless of sequence specificity, although it shows a higher affinity for the light- and heavy-strand promoters (LSP and HSP, respectively) (11, 30). In addition to these two HMG boxes, human TFAM has a linker region between the two HMG boxes and a carboxyl-terminal tail region (C-tail) composed of 27 and 25 residues, respectively (6).

* Corresponding author. Mailing address: Department of Clinical Chemistry and Laboratory Medicine, Kyushu University Graduate School of Medical Sciences, 3-1-1 Maidashi, Higashi-ku, Fukuoka 812-8582, Japan. Phone: 81-92-642-5749. Fax: 81-92-642-5772. E-mail: kang@mailserver.med.kyushu-u.ac.jp.

According to the strand-coupled model (4, 16, 38), replication of the L-strand, i.e., lagging-strand replication, occurs simultaneously with that of the H-strand. On the other hand, in another mtDNA replication model, the strand displacement model (34), replication of the nascent H-strand proceeds and displaces the parental H-strand until a replication origin of the L-strand, O_L, is exposed on a single strand. The process of mtDNA replication begins with the initiation of transcription at LSP. The transcript initiated from LSP forms an RNA-DNA hybrid at a replication origin for the H-strand, O_H. The RNA-DNA hybrid is processed to generate an RNA primer utilized by mitochondrial DNA polymerase γ (20). Thus, in the latter model, the replication of mammalian mtDNA is proposed to be coupled with transcription, and therefore TFAM is thought to be essential for replication of mtDNA (34). The role of transcription in the former model has not yet been clarified.

Abf2p, a TFAM homolog in *Saccharomyces cerevisiae*, has two HMG boxes and a short linker region between them, but unlike TFAM, it does not have a C-tail (12). Abf2p is abundant in mitochondria, with one Abf2p polypeptide present for every 15 bp of mtDNA (8). Disruption of the ABF2 gene leads to a loss of mtDNA and a resultant loss of respiratory competence when cells are grown in the presence of glucose. Expression of human TFAM in the *S. cerevisiae abf2* strain rescued the phenotype, implying a potential functional homology between human TFAM and Abf2p (30). However, unlike mammalian TFAM, Abf2p is not required for the initiation of transcription in yeast mtDNA (8). An in vitro transcription assay demonstrated that Abf2p or C-tail-deleted TFAM does not activate transcription, whereas a chimeric Abf2p containing the C-tail

does (6), suggesting that the C-tail of TFAM is necessary for transcriptional activation. This notion is also supported by a recent report that the C-tail of TFAM is necessary to bind mitochondrial transcription factor B (TFBM) and that this binding is required for transcription activation (24). In agreement with this, the import of full-length TFAM into isolated mitochondria increases transcription, but import of TFAM lacking the C-tail does not (14). Thus, the C-tail of TFAM is considered essential for the activation of transcription.

The mitochondrial nucleoids, protein-mtDNA complexes, have been studied extensively in the lower eukaryotes *S. cerevisiae* (17, 26) and *Physarum polycephalum* (32). In *S. cerevisiae* Abf2p is detected as a main component of the nucleoid and appears to function to maintain mtDNA and the nucleoid structure (17). In *P. polycephalum*, Glom, which also has two HMG boxes, shows a strong DNA-packaging activity (32). Both of these HMG family proteins can be functionally replaced by an *Escherichia coli* histone-like protein, HU (25, 32), implying that Abf2p and Glom package mtDNA.

There are several reports that mtDNA in higher eukaryotes is somewhat naked except for the D-loop region (2, 7, 29, 31), while the mtDNA of *Xenopus laevis* is reported to be packaged into regular beaded structures (3). These conflicting results on whether animal mtDNA takes on a higher nucleosome- or chromatin-like structure (mitochondrial nucleoid or mitochromatin/mitochondrial chromosome) are not fully resolved. Recent reports also suggest the existence of such a higher mtDNA structure in mammals (1, 13, 35). Because the amount of human TFAM is sufficient to cover the entire region of mtDNA (36) and because most TFAM molecules indeed bind to mtDNA (1), TFAM has been proposed to be one of the main components of the human mtDNA higher structure.

Homozygous gene disruption of *Tfam* is lethal in both mouse and chicken cells, at least in part due to mtDNA depletion and resultant loss of oxidative phosphorylation capacity (19, 22). In heterozygous cells, the expression of mouse and chicken TFAM was reduced by about 50% and the amount of mtDNA also decreased by about half (19, 22). These results suggest that TFAM is necessary to maintain mtDNA. There are two possibilities to explain mtDNA maintenance by TFAM. One is that, given that the replication of mtDNA is coupled to transcription (34), TFAM affects the replication of mtDNA directly. The other is that TFAM binds and stabilizes mtDNA, as do other HMG family proteins (5, 8, 12, 32, 39).

There have been no reports demonstrating overexpression of TFAM in mammalian cells. We established stable and inducible human cell lines overexpressing TFAM for the first time with a tetracycline-regulated gene expression system. In this study, with these TFAM-overexpressing cell lines and RNA interference (RNAi), we manipulated the amount of human TFAM in human HeLa cell lines and then analyzed mtDNA and mitochondrial transcription. We found that the amount of TFAM but not the transcription level is correlated to the amount of mtDNA.

MATERIALS AND METHODS

Antibodies. Antibodies to human TFAM, prohibitin, and BAP37 were produced by immunizing rabbits with recombinant glutathione *S*-transferase–human TFAM (28), glutathione *S*-transferase–prohibitin, and glutathione *S*-transferase–BAP37 proteins, respectively. Antibodies to cytochrome *b* and complex II were produced by immunizing rabbits with peptides of the C-terminal eight amino acids of cytochrome *b* and the C-terminal nine amino acids of the complex II iron sulfur protein, respectively (1). An antibody to human mitochondrial single-stranded DNA-binding protein (mtSSB) was described previously (36) as was an antibody to P32 (27). Antibodies against the hemagglutinin (HA) HA.11 epitope tag, cytochrome *c*, and calnexin were obtained from Covance, Stressgen, and Santa Cruz Biotechnology, respectively.

Preparation of tetracycline-regulated TFAM-overexpressing cell lines. To avoid suppression by RNAi, we introduced silent mutations in a human TFAM cDNA corresponding to the RNAi target in advance (from GTCTTGGCAAGT TGTCCAAAGAAACCTGTAAGTTCT to GTCTTAGCAAGTTGCCCTA AAAAGCCTGTAAGCTCT; the encoded amino acid sequence for both is VLASCPKKPVSS [amino acids 45 to 56]; sites where silent mutations have been introduced are in boldface) and named it pmod-TFAM. A DNA fragment encoding human TFAM lacking the C-terminal 25 amino acids (human TFAM-ΔC), i.e., it retained amino acids 1 to 221, was amplified with pMod-TFAM as a template. The sense primer contained a BamHI site, the Kozak sequence (18), and ATG for a first methionine in that order; the antisense primer contained an SpeI site. A DNA fragment specifying an HA tag was prepared by annealing the complementary synthesized oligonucleotides, which included, in order, the sequences for an SpeI restriction site, an HA epitope tag (11 amino acids), a stop codon, and an NheI site.

The DNA fragments for human TFAM and the HA tag were digested with appropriate restriction enzymes and inserted between the BamHI and NheI sites of vector pTRE2hyg (Clontech). This vector encodes the precursor human TFAM-ΔC with the HA tag at its C terminus and was named ph-TFAM-ΔC-HA. We also amplified a DNA fragment encoding precursor mouse TFAM (amino acids 1 to 243) by PCR, with a mouse cDNA library as a template with a sense primer (containing, in order, a BamHI site, the Kozak sequence [18], and ATG for a first methionine) and an antisense primer (containing an SpeI site). The mouse TFAM DNA fragment and the HA tag DNA fragment were inserted into the pTRE2hyg vector in the same way as the human construct (pm-TFAM-HA).

A HeLa Tet-Off cell line was obtained from Clontech. The cells were grown in Dulbecco's modified Eagle's medium (DMEM) with 10% fetal bovine serum (Gibco) and 100 μg of G418 per ml (Sigma). We transfected HeLa Tet-Off cells with our plasmids with the FuGene 6 reagent (Roche Molecular Biochemicals) and selected cells bearing the transgenes in the presence of G418 (400 μg/ml) (Wako), hygromycin B (200 μg/ml) (Wako), and doxycycline, a tetracycline derivative (1 μg/ml) (ICN Biomedicals). We isolated hygromycin-resistant clones, cultured them with or without doxycycline for about 10 days, and then examined the expression of recombinant proteins by Western blotting. These mouse and human TFAM-overexpressing cell lines were designated MTF (mouse TFAM full-length) and HΔC (human C-tail-deleted TFAM), respectively.

Suppression of human TFAM by RNAi. HeLa cells were grown in DMEM with 10% fetal bovine serum and antibiotics (100 μg of G418 per ml for control HeLa Tet-Off cells; 100 μg of G418 and 100 μg of hygromycin B per ml for MTF and HΔC cells) in 3.5-cm dishes. When the cells were about 50% confluent, the culture medium was replaced by 2 ml of DMEM containing 10% fetal bovine serum with and without doxycycline (1 μg/ml). The sequences of short interfering RNA (siRNA) duplexes were 5′-GUUGUCCAAAGAAACCUGUdTdT-3′ (sense siRNA) and 5′-ACAGGUUUCUUUGGACAACdTdT-3′ (antisense siRNA) (obtained from Qiagen); 12 μl of 20 μM siRNA duplexes was mixed with 200 μl of Opti-MEM (Gibco) in one tube; 12 μl of Oligofectamine (Invitrogen) was mixed with 48 μl of Opti-MEM in the other tube. The two mixtures were incubated for 10 min at room temperature and then combined and mixed gently by pipetting. The combined mixture was allowed to stand for another 20 min at room temperature. The siRNA-Oligofectamine mixture was then added to the cultured cells. After 24 h, the culture medium was replaced by new DMEM with 10% fetal bovine serum and appropriate antibiotics. When the cells were almost confluent, they were reseeded in two 3.5-cm dishes.

Western blotting. The cells from a 3.5-cm dish were collected in 1 ml of phosphate-buffered saline (PBS), and half of them were solubilized with 100 μl of sodium dodecyl sulfate (SDS) denaturing buffer consisting of 0.5% SDS and 1% 2-mercaptoethanol (the other half was used for mtDNA quantification [see below]). The mixture was briefly sonicated immediately after solubilization. Proteins were separated on an SDS–12% polyacrylamide gel by polyacrylamide gel electrophoresis (PAGE) and subsequently detected by immunoblotting. The signals were visualized with horseradish peroxidase-labeled anti-rabbit immunoglobulin G (Biosource) and ECL reagents (Amersham Biosciences). The chemiluminescence was recorded and quantified with a chilled charge-coupled device camera, LAS1000plus (Fuji).

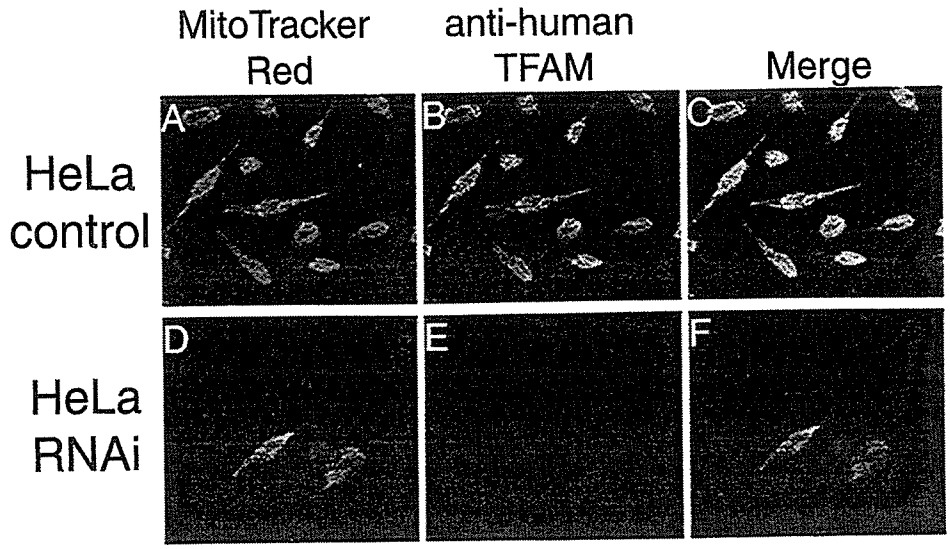

FIG. 1. Immunofluorescent images of HeLa cells treated by RNAi. Human TFAM in HeLa cells was identified with anti-human TFAM antibodies (B and E). Mitochondria were stained with MitoTracker Red (A and D). Panels C and F are merged images of panels A plus B and D plus E, respectively.

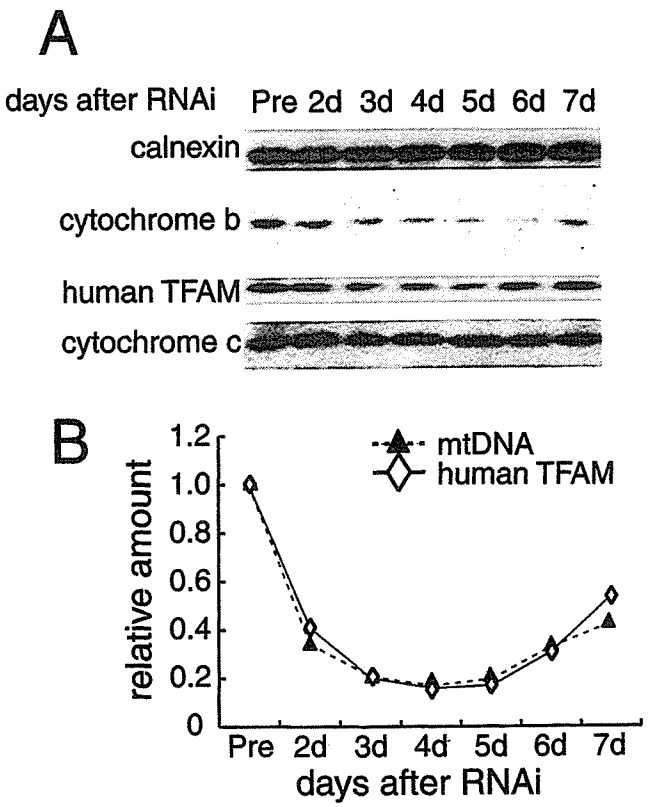

FIG. 2. Parallel decreases and increases in human TFAM and mtDNA after RNAi. (A) Calnexin (as a standard of cell amount), cytochrome *b*, human TFAM, and cytochrome *c* in HeLa cells were analyzed by Western blotting 2 to 7 days after RNAi. The relative amount of mtDNA was measured by quantitative PCR. (B) Representative daily changes in the relative amounts of human TFAM (◇) and mtDNA (▲).

Quantification of mtDNA. From the remaining half of the cells, total DNA was extracted with a DNeasy tissue kit (Qiagen). The total DNA was quantified with a PicoGreen double-stranded DNA quantitation kit (Molecular Probes). The relative amount of mtDNA was quantified by quantitative PCR with a LightCycler (Roche). The PCR mixture contained 2 ng of the total DNA (for a standard curve, 8, 4, 2, 1, and 0.5 ng of the total DNA were used), 10 pmol each of primers (5′-CCACCCAAGTATTGACTCACCC-3′ [nucleotides 16052 to 16073] and 5′-CGAGAAGGGATTTGACTGTAATG-3′ [nucleotides 16339 to 16361]) and 3 mM $MgCl_2$ in 20 μl. To estimate the amount of genomic DNA as an internal standard, a genomic beta-globin gene was amplified in a 20-μl reaction mixture containing 16 ng of the total DNA (for a standard curve, 64, 32, 16, 8, and 4 ng of the total DNA were used), 10 pmol each of primers (5′-CTGCCCTGTGGG GCAAGGTGAACGTGGATG-3′ and 5′-CAGGTGAGCCAGGCCATCACT AAAGGCACC-3′), and 3 mM $MgCl_2$. The amount of mtDNA was adjusted to the amount of genomic DNA.

Immunofluorescent imaging of HeLa cells. Cells were incubated in the presence of 100 nM MitoTracker Red CMXRos (Molecular Probes) for 20 min. After washing with PBS three times, the cells were fixed with acetone-methanol (50:50, vol/vol) for 5 min. After washing with PBS three times, the fixed cells were blocked with bovine serum albumin-PBS (1% bovine serum albumin in PBS) for 30 min, then incubated with 250-fold-diluted anti-human TFAM antiserum or anti-HA antibody in bovine serum albumin-PBS for 1 h. After washing the cells with wash buffer (0.1% Tween 20 in PBS) three times, cells were incubated with 250-fold-diluted Alexa Fluor 488 goat anti-rabbit immunoglobulin G (Molecular Probes) for 30 min. Fluorescence images were taken with a confocal laser microscope (Bio-Rad Laboratories).

Isolation of mitochondria from HeLa cells. All procedures were done at 4°C. HeLa cells cultured in 10-cm dishes were scraped with a cell lifter (Costar) into 3 ml of PBS, pelleted by centrifugation, and washed with homogenization buffer (10 mM HEPES-KOH, pH 7.4, and 0.25 M sucrose). The cells were suspended in 4 volumes of the buffer and homogenized with a Potter-Elvehjem homogenizer. The homogenate was centrifuged at 900 × *g* for 10 min to remove the unbroken cells and nuclei. The supernatant was centrifuged at 10,000 × *g* for 6 min. The pellet was collected as a crude mitochondrial fraction and used for in organello transcription assays or for preparing Nonidet P-40-insoluble fractions.

In vitro transcription assay. The cDNA coding for mature human TFAM (amino acid residues 42 to 246) and mature human TFAM-ΔC-HA (amino acid residues 42 to 221 and C-terminal HA tag) were inserted into the pProEXHTb vector (Gibco). The recombinant His-human TFAM and His-human TFAM-ΔC-HA were expressed in *Escherichia coli* BL21 cells and purified Ni^{2+}-bound chelating Sepharose resin (Amersham Biosciences) as described previously (28, 36). In vitro transcription reactions were performed with a cloned DNA fragments corresponding to nucleotides 1 to 477 of human mtDNA as previously described (10).

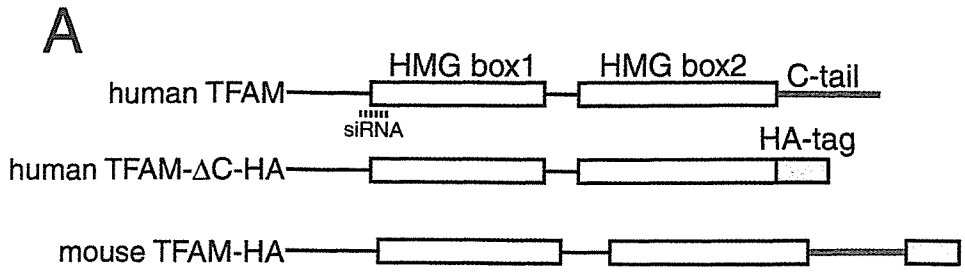
A
human TFAM
HMG box1
HMG box2
C-tail
siRNA
human TFAM-ΔC-HA
HA-tag
mouse TFAM-HA

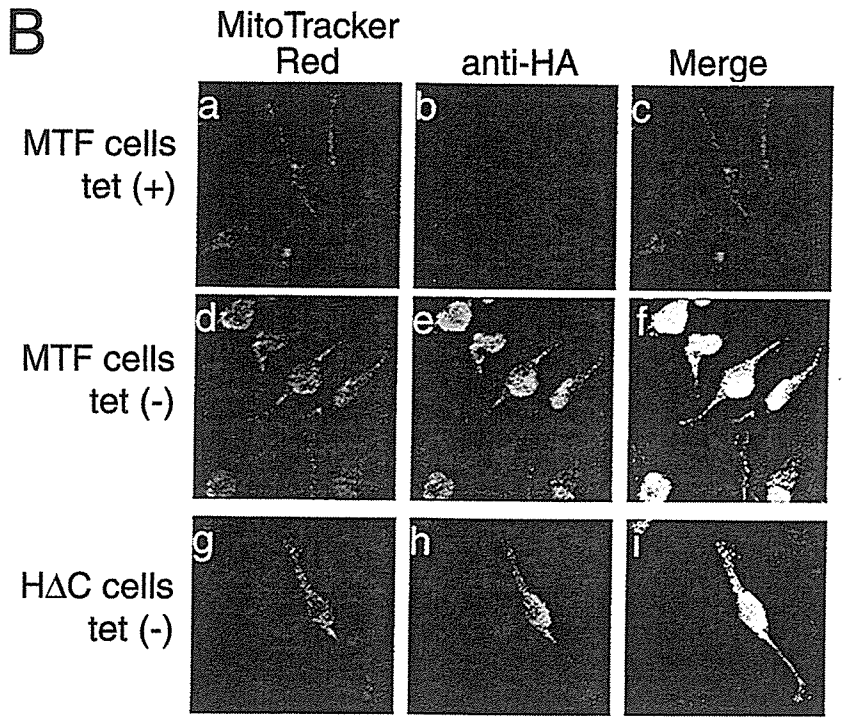
B
MitoTracker Red
anti-HA
Merge
MTF cells tet (+)
MTF cells tet (-)
HΔC cells tet (-)
a
b
c
d
e
f
g
h
i

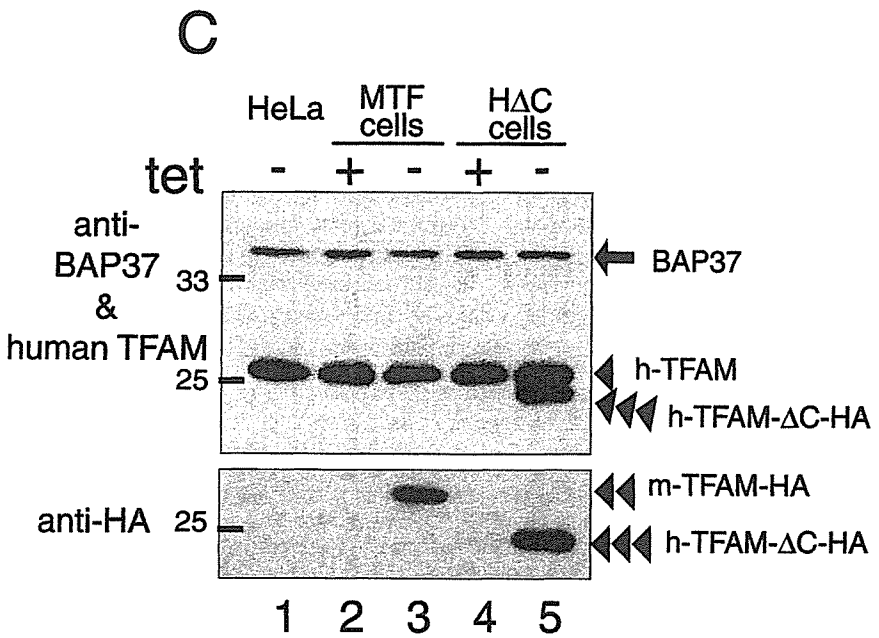
C
HeLa
MTF cells
HΔC cells
tet
- + - + -
anti-BAP37 & human TFAM
33
25
BAP37
h-TFAM
h-TFAM-ΔC-HA
anti-HA
25
m-TFAM-HA
h-TFAM-ΔC-HA
1 2 3 4 5

In organello transcription assay. In organello transcription was measured by the method of Enriquez et al. with slight modifications (9). The mitochondrial fraction was resuspended in transcription buffer (10 mM Tris-HCl [pH 7.4], 25 mM sucrose, 75 mM sorbitol, 100 mM KCl, 10 mM K_2HPO_4, 50 μM EDTA, 5 mM $MgCl_2$, 1 mM ATP, 1 mg of bovine serum albumin per ml). Mitochondria (200 μg of protein) were incubated in 300 μl of the transcription buffer containing 10 μCi of [α-^{32}P]UTP (Amersham Biosciences) at 37°C for 30 min. After the incubation, the mitochondria were pelleted at 15,000 × *g* for 1 min and then washed with nuclease buffer (0.25 M sucrose, 10 mM Tris-HCl [pH 8.0], 1 mM $CaCl_2$). The mitochondria were resuspended in 400 μl of nuclease buffer with 100 units of nuclease S7 (Roche Molecular Biochemicals) and incubated at room temperature for 20 min. The mitochondria were then pelleted at 15,000 × *g* for 1 min and washed with TES buffer (10 mM Tris-HCl [pH 7.4], 1 mM EDTA, 0.25 M sucrose). The mitochondrial pellet was solubilized in 100 μl of lysis buffer (50 mM Tris-HCl [pH 8.0], 20 mM NaCl, 1 mM EDTA, 1% SDS) containing 20 μg of protease K (Gibco) and incubated at room temperature for 15 min. After addition of 100 μl of a phenol-chloroform-isoamyl alcohol mixture (25:25:1, vol/vol/vol) and vortexing for 1 min, the mixture was centrifuged at 20,000 × *g* for 5 min, and 80 μl of the aqueous phase was transferred to a clean tube. Then 1 μl of Pellet Paint (Novagen), 80 μl of 3 M sodium acetate (pH 5.2), and 300 μl of ethanol were added, and the mitochondrial nucleic acids were precipitated. The pellets were solubilized with sample buffer (99% formamide, 1 mM EDTA, and bromphenol blue) and incubated at 95°C for 3 min. DNA size makers (100-bp DNA ladder and 1-kb DNA ladder, New England BioLabs) were [γ-^{32}P]ATP labeled with Ready-To-Go T4 polynucleotide kinase (Amersham Biosciences). Samples were separated on an 8 M urea–4% polyacrylamide gel by electrophoresis and analyzed with a BAS-2500 (Fuji). The isolated mitochondria (5 μg) were analyzed by Western blotting to check the amount of mitochondria and efficiency of RNAi.

Separation of mitochondrial NP-40-soluble and -insoluble fractions. The mitochondria were resuspended in TES buffer containing 0.5% NP-40 and 1 mM dithiothreitol (0.5 mg of protein/ml) and incubated for 30 min on ice with intermittent mixing. The mitochondria were centrifuged at 20,000 × *g* for 30 min and separated into a pellet (P1) and a supernatant (S1). The P1 fraction (10 μg of protein) was resuspended with 20 μl of nuclease buffer (10 mM Tris-HCl [pH 7.4], 0.25 M sucrose, 1 mM dithiothreitol, 2.5 mM $CaCl_2$, and 0.5% NP-40) and incubated for 30 min on ice with 2.5 U of nuclease S7 or 0.5 μg of RNase A (DNase free; Wako). After centrifugation at 20,000 × *g* for 30 min, the sample was separated into a pellet (P2) and a supernatant (S2). Proteins from each fraction were separated by SDS-PAGE and subsequently analyzed by Western blotting with appropriate primary antibodies.

mtDNA in the P1 and S1 fractions was detected by PCR as described previously (1). Briefly, total mitochondria, P1, and S1 (from 10 μg of mitochondria) were incubated at 95°C for 30 min with 0.5 μg of protease K (Gibco) and diluted in 200 μl of distilled water. With 1 μl each of the diluted samples, a fragment of mtDNA was amplified with PCR primers (nucleotides 16052 to 16073 and nucleotides 16339 to 16361) and Ex-taq DNA polymerase (Takara). The number of amplification cycles was 25, and the PCR products were separated on a 1% agarose gel.

RESULTS

Reduced expression of human TFAM by RNAi. To observe a dose effect of TFAM, we downregulated the expression of human TFAM by RNAi in HeLa cells. Three days after RNAi treatment, human TFAM was barely detectable on immunofluorescent images with anti-human TFAM antibodies (compare Fig. 1B and E). To monitor the change in the levels of human TFAM and other mitochondrial proteins, cells were collected daily between days 2 and 7 and analyzed by Western blotting (Fig. 2A). The amount of human TFAM was decreased maximally at days 3 and 4 and then gradually increased again (Fig. 2A, third panel). The amounts of calnexin, a microsomal protein, and cytochrome *c*, a nucleus-encoded mitochondrial protein, did not change (Fig. 2A, top and bottom panels). The amounts of several other nucleus-encoded mitochondrial proteins (prohibitin, BAP37, and VDAC) were not affected by this RNAi (data not shown), confirming the specificity of the RNAi treatment. The reduction in cytochrome *b*, an mtDNA-encoded protein (Fig. 2A, second panel), probably resulted from a decrease in mtDNA (Fig. 2B). We measured the relative amount of mtDNA by quantitative PCR and found that the amount fell and rose in parallel with that of human TFAM (Fig. 2B). The levels of human TFAM and mtDNA were 0.141 ± 0.052 and 0.132 ± 0.061 (n = 4) of those of control cells at day 3. Thus, the amount of mtDNA was strongly correlated with the amount of TFAM in vivo.

Preparation of tetracycline-regulated TFAM-overexpressing cell lines. Conversely, to see whether an increase in TFAM would affect the amount of mtDNA, we created TFAM-overexpressing cell lines. We made two kinds of Tet-Off gene expression vectors, ph-TFAM-ΔC-HA and pm-TFAM-HA, in order to express C-tail-deleted human TFAM with an HA tag and mouse full-length TFAM with an HA tag, respectively (Fig. 3A). To produce the stable TFAM-expressing cell lines, we transfected HeLa Tet-Off cells with each vector and cultured them with hygromycin for selection and with doxycycline to suppress expression. We isolated hygromycin-resistant colonies and checked the expression of TFAM by Western blotting after culturing for 10 days without doxycycline. Fourteen of 24 hygromycin-resistant ph-TFAM-ΔC-HA-transfected clones expressed high levels of human TFAM-ΔC-HA (about 50 to 120% compared with the amount of endogenous human TFAM). Thirteen of 24 hygromycin-resistant pm-TFAM-HA-transfected clones expressed high levels of mouse TFAM-HA (about 50 to 140% compared with the amount of endogenous human TFAM). These mouse TFAM- and human TFAM-ΔC-overexpressing cell lines were designated MTF (mouse TFAM full-length) and HΔC (human C-tail-deleted TFAM), respectively.

When cultured without doxycycline, immunofluorescent imaging of MTF cells with anti-HA antibodies showed granular fluorescence. This pattern colocalized with that of MitoTracker Red, a mitochondrion-staining fluorescent dye (Fig. 3B, panels d to f), indicating that the expressed exogenous TFAM localized to mitochondria, while the cells cultured with doxycycline showed almost no fluorescence with anti-HA an-

FIG. 3. Tetracycline-regulated expression of TFAM. (A) The scheme of recombinant TFAM molecules. Human and mouse TFAM have two HMG boxes (white square) and a C-tail region (gray bar). An HA.11 epitope tag is indicated by a gray square. The position of the RNAi target is indicated by a dotted line. (B) MTF cells and HΔC cells were cultured with doxycycline [tet (+)] or without doxycycline [tet (−)]. Mitochondria were stained with MitoTracker Red (panels a, d, and g), and recombinant TFAM was stained with anti-HA antibodies (panels b, e, and h). The merged images are shown in panels c, f, and i. (C) Western blotting analysis of TFAM molecules. Total cell lysates were used for Western blotting. BAP37 (arrow) is shown as an internal standard for the amount of protein applied in the samples. Antibodies for BAP-37 and human TFAM were added together for detecting the two proteins (upper panel). Then the membrane was reprobed with anti-HA antibody (lower panel). Endogenous human TFAM (arrowhead), exogenous mouse TFAM-HA (double arrowheads), and exogenous human TFAM-ΔC-HA (triple arrowheads) are indicated.